Multiple renal cysts and dilated calyces in $Taz^{lacZ/lacZ}$ mice. To characterize the phenotype that may be related to early mortality, we performed macroscopic and histological examinations on surviving $Taz^{lacZ/lacZ}$ mice. The most prominent abnormalities were first detected in the kidneys. Adult $Taz^{lacZ/lacZ}$ mice showed bilaterally enlarged, pale kidneys (Fig. 2, *C* and *D*). The calyces were extremely dilated, leaving thinned parenchyma containing multiple cysts (Fig. 2*E*). Histological analysis of 10-wk-old $Taz^{lacZ/lacZ}$ mice demonstrated numerous cysts of various sizes replacing most of the renal parenchyma (Fig. 2*G*), whereas no such changes were found in wild-type and $Taz^{+/lacZ}$ kidneys (Fig. 2, *F* and *H*). Cysts were lined by a flattened epithelial monolayer and sometimes contained a glomerular tuft, indicating an origin from Bowman's capsule (Fig. 2, *G* and *I*). The surrounding tissues showed increased interstitial fibrosis in Masson's trichrome staining (data not shown). Notably, these renal changes in $Taz^{lacZ/lacZ}$ mice shared a similar histology to human PKD.

In contrast, calyceal dilatation is uncommon in human PKD. To examine whether the dilation of the pelvis and atrophy of the medulla in $Taz^{lacZ/lacZ}$ kidneys could be secondary to anatomical obstruction in the urinary tract, we injected black ink into the pelvis of *embryonic day 18.5* kidneys. In $Taz^{lacZ/lacZ}$ kidneys, peristaltic passage of urine through the ureter was observed similar to wild-type and heterozygous littermates (data not shown). The urinary bladder was not apparently dilated in $Taz^{lacZ/lacZ}$ embryos at this stage (data not shown). These results suggested that the hydronephrotic changes in $Taz^{lacZ/lacZ}$ kidneys were not due to mechanical obstruction of the urinary tract.

Extrarenal phenotypes in $Taz^{lacZ/lacZ}$ mice. In human ADPKD, extrarenal manifestations are often observed in the liver, pancreas, blood vessels, heart, and other organs. However, examination of adult $Taz^{lacZ/lacZ}$ mice did not reveal obvious abnormalities in these tissues (data not shown). Instead, the lung was unexpectedly affected in $Taz^{lacZ/lacZ}$ mice. Histological examination revealed enlarged air spaces in $Taz^{lacZ/lacZ}$ lungs at the age of 8–9 mo (Fig. 3, *A* and *B*). The mean linear intercept, as a measure of interalveolar wall distance, was significantly greater in $Taz^{lacZ/lacZ}$ mice (149.6 ± 11.5 μm, $n = 4$) than in wild-type mice (51.6 ± 2.1 μm, $n = 4$) (Fig. 3*C*). There were no findings indicative of increased inflammation or fibrosis in $Taz^{lacZ/lacZ}$ lungs. The phenotype of $Taz^{lacZ/lacZ}$ lungs is highly reminiscent of human pulmonary emphysema.

The changes in the kidney and lung were observed in all the homozygous mice derived from two independent recombinant ES clones, although the severity of symptoms varied among individuals. In contrast, no wild-type and $Taz^{+/lacZ}$ mice displayed abnormalities (Figs. 2, *A* and *B*, and 3*A*).

Urinary concentration defects in $Taz^{lacZ/lacZ}$ mice. In addition to multiple cysts and dilated calyces, $Taz^{lacZ/lacZ}$ mice showed signs of polyuria. Indeed, the urinary bladder in $Taz^{lacZ/lacZ}$ mice was typically distended with a large volume of urine (data not shown). Measurement of the 48-h urine frequency and volume revealed that urine volume per void and total volume per day were much higher in $Taz^{lacZ/lacZ}$ mice than in $Taz^{+/lacZ}$ mice (Fig. 4). Measurements of urinary parameters showed polyuria and concentrating defects in $Taz^{lacZ/lacZ}$ mice, as indicated by lower urinary osmolality (Table 2). Overall electrolyte excretion was not enhanced, although excretion of chloride was slightly increased (Table 2), indicating that electrolyte reabsorption remained grossly preserved. Urinary albumin excretion in $Taz^{lacZ/lacZ}$ mice appeared to be increased, although the difference was not statistically significant (Table 2). The polyuria and concentrating defects in $Taz^{lacZ/lacZ}$ mice were not improved by vasopressin administration (data not shown), suggesting that the abnormalities were likely to be nephrogenic rather than due to vasopressin deficiency. Overall, $Taz^{lacZ/lacZ}$ kidneys were characterized by the concomitant occurrence of features that are typical of human PKD, including multicystic formation and urinary concentrating defects, and atypical features such as calyceal dilatation and hydronephrosis.

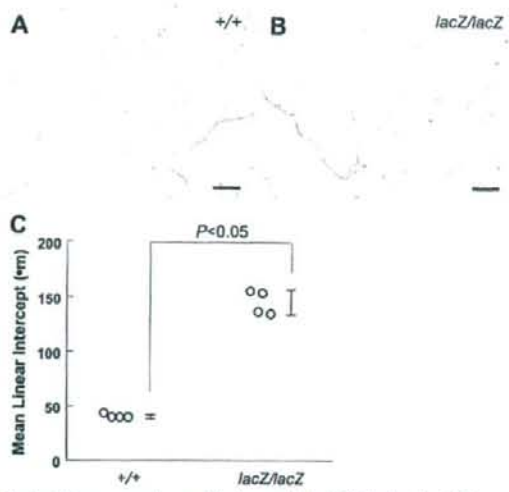

Fig. 3. Pulmonary emphysema-like changes in $Taz^{lacZ/lacZ}$ mice. *A* and *B*: hematoxylin and eosin staining of lung sections of $Taz^{+/+}$ (*A*) and $Taz^{lacZ/lacZ}$ (*B*) mice aged 9 mo. Enlarged air spaces and alveolar wall disruption are observed in the lung of $Taz^{lacZ/lacZ}$ mice. Scale bars indicate 100 μm. *C*: morphometric analysis. Mean linear intercept values are significantly greater in $Taz^{lacZ/lacZ}$ mice ($n = 4$) than wild-type mice ($n = 4$) aged 8–9 mo. A total of 288 lines drawn across the lung section were analyzed for each group. Error bars indicate SDs of the mean.

Cysts primarily originated from glomeruli and proximal tubules in $Taz^{lacZ/lacZ}$ embryos. To determine the time point at which cysts first arose in the kidneys of $Taz^{lacZ/lacZ}$ embryos, we performed histological analysis on kidneys at different embryonic stages. At *embryonic day 13.5*, the branching of ureteric buds and the initial formation of renal vesicles and comma- and S-shaped bodies appeared to be normal in both $Taz^{lacZ/lacZ}$ and wild-type kidneys (Fig. 5, *A* and *B*). At *embryonic day 15.5*, morphological abnormalities were first detected as dilatation of the Bowman's capsules and adjacent tubules in $Taz^{lacZ/lacZ}$ embryos (Fig. 5, *C* and *D*).

At *embryonic day 18.5*, $Taz^{lacZ/lacZ}$ kidneys exhibited tubules with varying degrees of dilatation and multiple cysts in inner cortical and medullary regions (Fig. 5, *E* and *F*). Cyst-lining epithelial cells appeared heterogeneous in morphology; some were flattened and others were rather cuboidal (Fig. 5, *G* and *H*). Glomerular tufts were detected in a small subset of cysts at this stage (Fig. 5, *G* and *H*). The renal pelvis was dilated, and the medulla was atrophic with disturbed formation of the papilla (Fig. 5, *E* and *F*). In contrast, the nephrogenic zone

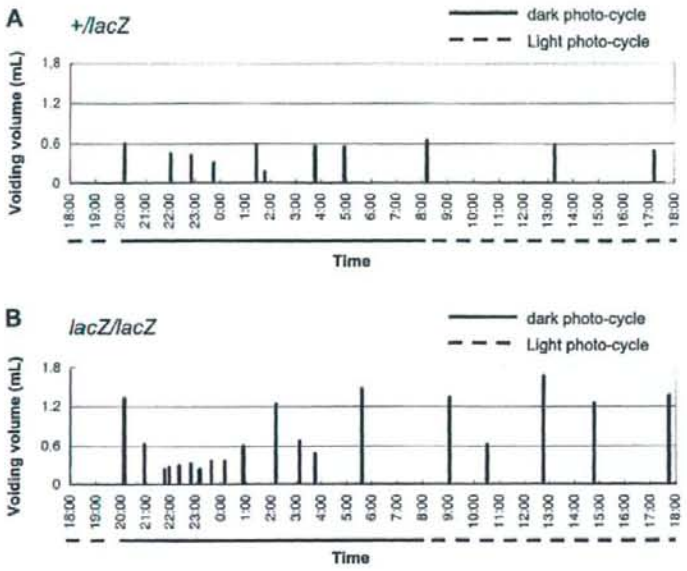

Fig. 4. Representative 24-h urinary frequency/volume records. Mice aged 5–6 mo were subjected to the analysis. Urine volume per void, voiding frequency, and total volume per day are greatly increased in $Taz^{lacZ/lacZ}$ mice (*B*) compared with $Taz^{+/lacZ}$ mice (*A*).

was well-developed in the outer cortex just beneath the capsule and contained many developing nephrons in $TAZ^{lacZ/lacZ}$ and wild-type kidneys (Fig. 5, *E–H*).

We examined the origins of the cysts using segment-specific markers. LTA, a lectin specific for the proximal tubule, stained the majority of epithelial cells lining dilated tubules and cysts in *embryonic day 18.5* $Taz^{lacZ/lacZ}$ embryos (Fig. 6, *A–D*). In contrast, no cysts were stained with DBA, a lectin specific for the collecting duct, at the same stage (Fig. 6, *E–H*). These results suggested that the cystic changes in $Taz^{lacZ/lacZ}$ kidneys primarily originated from glomeruli and proximal tubules during the maturation of induced nephrons.

Expression of Taz in developing kidneys. To correlate the renal phenotype of $Taz^{lacZ/lacZ}$ mice with *Taz* expression, we first performed in situ hybridization on wild-type embryonic kidneys. At *embryonic day 14.5*, *Taz* transcripts were diffusely expressed in both mesenchymal and epithelial cells in the developing metanephros (Fig. 7, *A* and *B*). *Taz* was also present in the ureteric bud (Fig. 7, *A* and *B*). At *embryonic day 16.5*, *Taz* was expressed in mesenchymal and epithelial cells in the nephrogenic zone and collecting ducts (Fig. 7, *C* and *D*).

In contrast to in situ hybridization, β-galactosidase activity was observed only in limited cell populations. At *embryonic day 16.5* and *day 0* postpartum, $Taz^{+/lacZ}$ kidneys exhibited sporadic *lacZ* expression in glomeruli and capillary endothelial cells that were positive for CD31 (Fig. 7, *E*, *F*, and *J–L*), indicating that *lacZ* expression may only reflect a part of the authentic *Taz* expression, possibly due to disruption of critical genomic sequences. In $Taz^{lacZ/lacZ}$ homozygous kidneys, β-galactosidase activity was detected in stromal(-like) cells, especially in the outer cortical region as well as in glomeruli and capillary endothelial cells (Fig. 7, *G–I*, *M*, and *N*). In addition, some cysts are lined by *lacZ*-positive cells in *day 0* postpartum $Taz^{lacZ/lacZ}$ kidneys (Fig. 7*O*).

Expression of cystic disease transcripts and proteins in $Taz^{lacZ/lacZ}$ *kidneys.* To find clues to the mechanism underlying the renal phenotype of $Taz^{lacZ/lacZ}$ mice, we analyzed the expression of genes involved in human PKD. No alterations in the levels of *Pkd1* and *Pkd2* mRNA and their products, polycystin-1 and polycystin-2, were observed at *embryonic day 15.5* and *18.5* by real-time RT-PCR (Fig. 8, *A* and *B*) and Western blotting (Fig. 8*D*). Also, the expression of *Pkhd1*, a gene linked to ARPKD, was not different between wild-type and $Taz^{lacZ/lacZ}$ kidneys (Fig. 8*C*). These results indicated that renal cyst formation induced by *Taz*-null mutation was not due to changes in the expression of *Pkd1*, *Pkd2*, and *Pkhd1* at the perinatal stage.

Expression of genes involved in water metabolism in $Taz^{lacZ/lacZ}$ *kidneys.* The absence of changes in the expression of cystic disease genes and concomitant diabetes insipidus-like state led us to speculate that unique pathogenetic mechanisms might

Table 2. *Defects in urinary concentration in Taz/lacZ/lacZ mice*

	Taz+/+	*Taz/lacZ/lacZ*
n	6	6
Age, wk	20–26	20–26
Body wt, g	36.8±2.1	29.4±3.1*
Water intake, ml/day	6.7±1.4	17.5±2.4*
Urine volume, ml/day	3.56±1.39	10.76±3.02*
Osmolality, mosmol/kgH_2O	2,765±646	855±131*
Urine nitrogen, mg·day^{-1}·g body wt^{-1}	4.11±0.84	3.29±1.36
Creatinine, g·day^{-1}·g body wt^{-1}	32.3±7.0	34.5±13.3
Albumin, g·day^{-1}·g body wt^{-1}	1.91±1.02	29.60±42.49
Na^+, meq·day^{-1}·g body wt^{-1}	0.011±0.004	0.011±0.002
K^+, meq·day^{-1}·g body wt^{-1}	0.034±0.007	0.035±0.009
Cl^-, meq·day^{-1}·g body wt^{-1}	0.017±0.003	0.022±0.006†

Values are means ± SD. *$P < 0.01$ and †$P < 0.05$.

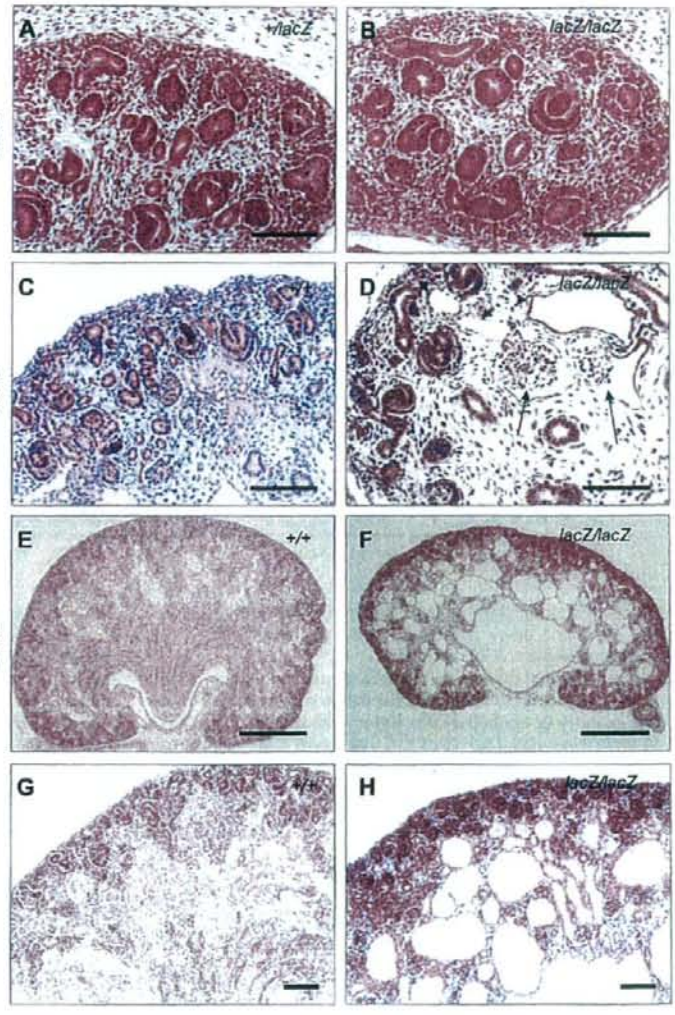

Fig. 5. Histological examination of developing kidneys in control (*A*, *C*, *E*, and *G*) and $Taz^{lacZ/lacZ}$ (*B*, *D*, *F*, and *H*) embryos. *A* and *B*: at *embryonic day 13.5*, branching of ureteric buds and formation of renal vesicles and comma- and S-shaped bodies are observed in $Taz^{lacZ/lacZ}$ (*B*) as well as wild-type and $Taz^{+/lacZ}$ (*A*) kidneys. *C* and *D*: at *embryonic day 15.5*, dilatation of Bowman's capsules (arrows) and adjacent tubules (arrowheads) are detected in $Taz^{lacZ/lacZ}$ kidneys (*D*) but not in wild-type kidneys (*C*). *E–H*: at *embryonic day 18.5*, the atrophic medulla contains multiple cysts of various sizes in $Taz^{lacZ/lacZ}$ kidneys (*F* and *H*). The pelvis is dilated and the papilla is not well formed (*F*). These changes are not observed in wild-type kidneys (*E* and *G*). The nephrogenic zone is present in the outer cortex just beneath the capsule in $Taz^{lacZ/lacZ}$ (*H*) and wild-type (*G*) kidneys. Scale bars indicate 100 μm (*A–D*, *G*, and *H*) and 500 μm (*E* and *F*).

underlie the renal phenotypes in $Taz^{lacZ/lacZ}$ kidneys. To explore the basis for disturbed water metabolism, we investigated the expression of genes and proteins that are involved in renal water transport. Although the urinary concentration defects in $Taz^{lacZ/lacZ}$ mice were resistant to exogenous vasopressin, real-time RT-PCR analysis showed that the expression of the arginine vasopressin receptor 2 gene (*Avpr2*) was largely unaffected in $Taz^{lacZ/lacZ}$ kidneys (Fig. 9*A*). The expression of aquaporin (*Aqp-1*, *-2*, and *-3*) water channels that are involved in renal water reabsorption (28) was not different among wild-type, heterozygous, and homozygous mutant kidneys (Fig. 9*B*). Immunostaining demonstrated that aquaporin-3 was localized in the basolateral membrane of epithelial cells in both $Taz^{lacZ/lacZ}$ and control $Taz^{+/lacZ}$ kidneys (Fig. 9, *C* and *D*), indicating that the polarity of aquaporin-3 localization in $Taz^{lacZ/lacZ}$ epithelial cells was intact. In $Taz^{lacZ/lacZ}$ kidneys, aquaporin-3 was expressed in many noncystic tubules and a few cysts (Fig. 9*D*), indicating an origin from the renal collecting ducts. Aquaporin-2 was also expressed similarly in collecting ducts in heterozygous and homozygous kidneys at *embryonic day 18.5* (Fig. 9, *E* and *F*). These results indicated that the renal phenotype of $Taz^{lacZ/lacZ}$ mice was not caused by changes in the expression of *Avpr2* or aquaporins.

DISCUSSION

In the present study, we demonstrate that a null mutation of *Taz* results in the formation of bilateral multicystic kidneys and

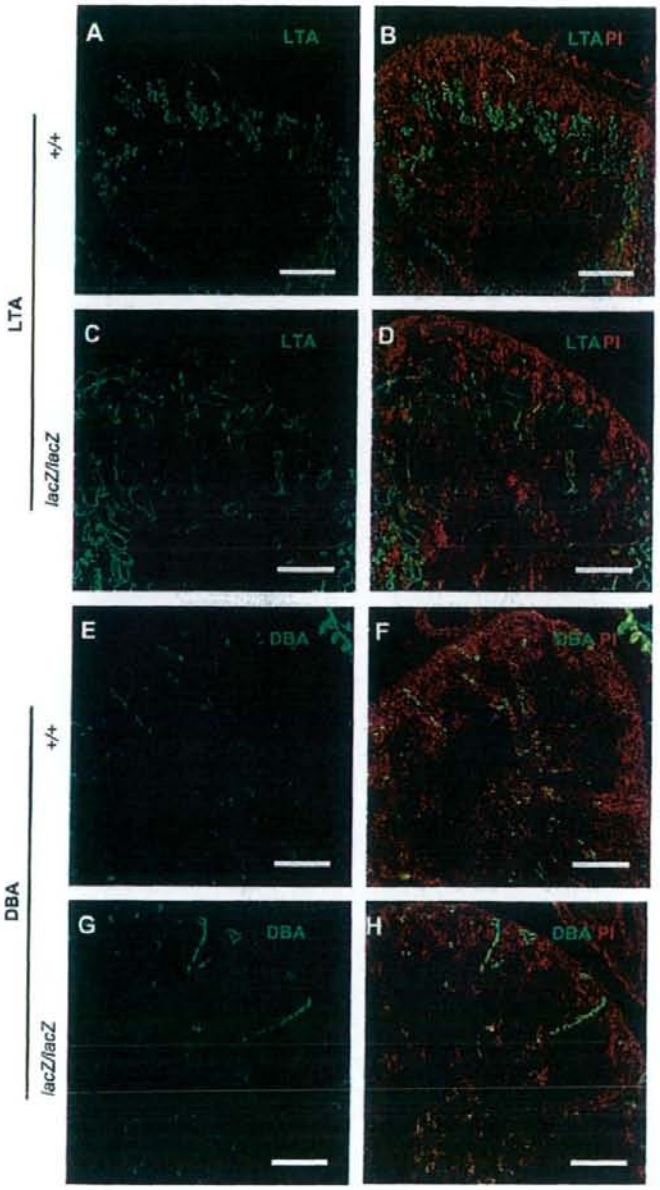

Fig. 6. Proximal tubular dilatation leading to cyst formation in $Taz^{lacZ/lacZ}$ embryos. Sections were stained with *Lotus tetragonolobus* agglutinin (LTA; *A–D*) or *Dolichos biflorus* agglutinin (DBA; *E–H*) in wild-type (*A*, *B*, *E*, and *F*) and $Taz^{lacZ/lacZ}$ (*C*, *D*, *G*, and *H*) kidneys at *embryonic day 18.5*. *B*, *D*, *F*, and *H* show costaining with propidium iodide and lectins. Epithelial cells lining dilated tubules and cysts stain positive with LTA but not with DBA in $Taz^{lacZ/lacZ}$ kidneys. Scale bars indicate 250 μm.

diffuse emphysematous changes in the lung. Renal cysts mainly originate from the glomeruli and proximal tubules around *embryonic day 15.5*, as revealed by histological features and lectin marker staining. Later, the renal changes are accompanied by pelvic dilatation and atrophy of the medulla, indicating hydronephrosis. After birth, only one-fifth of TAZ-deficient homozygotes grow to adulthood. The early mortality may be due to water and electrolyte imbalance and/or respiratory insufficiency. Surviving mutants demonstrate progressive renal changes with massive polyuria. The renal phenotype of

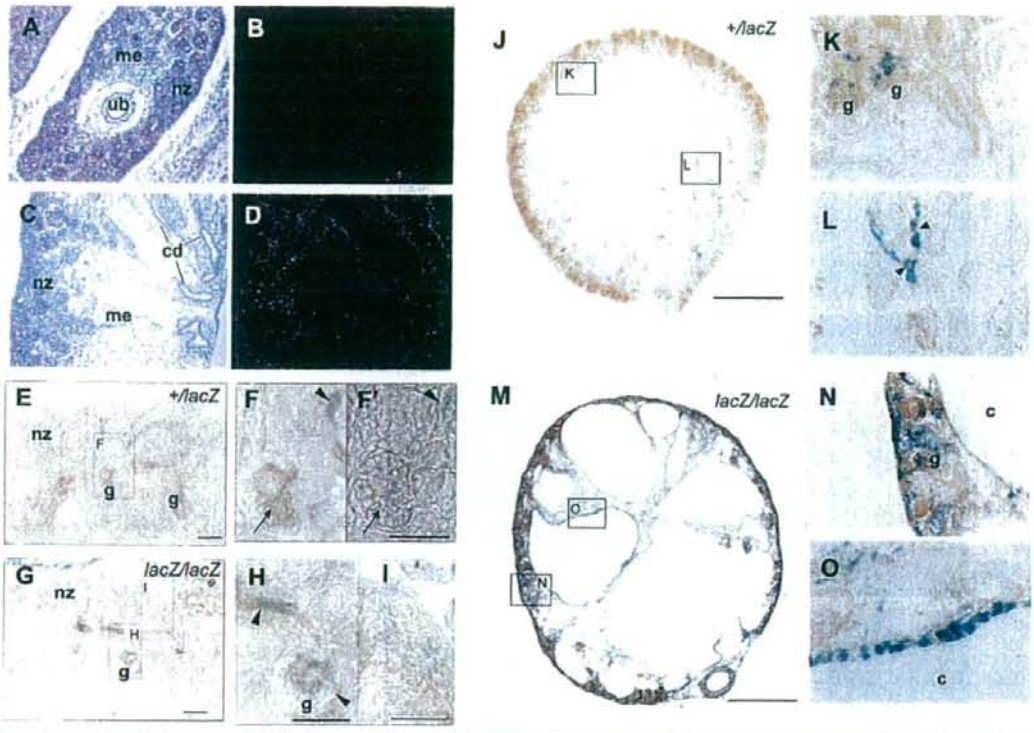

Fig. 7. *Taz* expression during metanephric development. *A–D*: in situ hybridization of mouse embryonic kidneys with probes for *Taz*. Brightfield (*A* and *C*) and darkfield (*B* and *D*) images of *embryonic day 14.5* (*A* and *B*) and *embryonic day 16.5* (*C–F*) kidneys are shown. *A* and *B*: at *embryonic day 14.5*, *Taz* transcripts are diffusely detected in metanephric mesenchymal and epithelial cells and the ureteric bud. *C* and *D*: at *embryonic day 16.5*, *Taz* is expressed in mesenchymal and epithelial cells in the nephrogenic zone. *Taz* is also expressed in the collecting ducts. *E–O*: β-galactosidase activity in $Taz^{+/lacZ}$ (*E*, *F*, and *J–L*) and $Taz^{lacZ/lacZ}$ (*G–I* and *M–O*) kidneys at *embryonic day 16.5* (*E–I*) and *day 0* postpartum (P0; *J–O*). *E*, *F*, and *F'*, in *embryonic day 16.5* $Taz^{+/lacZ}$ kidneys, X-gal staining (blue) is observed in glomeruli (arrows) and CD31-stained (brown) capillary endothelial cells (arrowheads). X-gal staining with (*F*) and without (*F'*) CD31 staining is shown. *G–I*: in *embryonic day 16.5* $Taz^{lacZ/lacZ}$ kidneys, X-gal staining is observed in stromal(-like) cells (open arrowheads in *I*) as well as in glomeruli and capillary endothelial cells (filled arrowheads in *H*). *J–L*: in P0 $Taz^{+/lacZ}$ kidneys, scattered X-gal staining is observed in glomeruli (*K*) and capillary endothelial cells (*L*). *M–O*: in P0 $Taz^{lacZ/lacZ}$ kidneys, X-gal staining is observed in outer cortical stromal cells, glomeruli, and capillaries (*N*). Some cysts are lined by X-gal-positive cells (*O*). Sections of P0 kidney were counterstained with Orange G. c, cyst; cd, collecting duct; g, glomerulus; me, mesenchyme; nz, nephrogenic zone; ub, ureteric bud. Scale bars indicate 50 μm (*E* and *I*) and 500 μm (*J* and *M*).

TAZ-deficient mice is reminiscent of human renal cystic diseases, as represented by PKD, but is distinct in that it manifests as severe hydronephrosis and urinary concentration defects.

Comparison of the renal phenotype of TAZ-deficient mice to human cystic kidney diseases. In human ADPKD, the epithelial-lined cysts originate from any segment of the nephron and collecting ducts, and in ARPKD the cysts mainly originate from the collecting ducts (3, 10). In contrast, the cysts in TAZ-deficient kidneys mainly originate from the glomeruli and proximal tubules. However, patients with early onset ADPKD may develop glomerular cysts, suggesting that cyst formation in the proximal nephrons may be an early manifestation of ADPKD (11, 15). Consistently, *Pkd1*-null mice start to exhibit cyst formation at *embryonic day 15.5* in the proximal tubule (20). Other animal models of PKD, such as the *cpk/cpk* mice and the Han:SPRD *cy/+* rats, have also shown cysts originating predominantly from the proximal tubule (39). Studies of human fetuses with ARPKD have shown cysts originating from proximal tubules. Thus the renal phonotype of TAZ-deficient mice may recapitulate the early phase of human PKD.

However, no apparent differences in the expression of PKD genes, *Pkd1*, *Pkd2*, and *Pkhd1*, are detected in the kidneys of wild-type and TAZ-deficient embryos before birth. This finding indicates that cyst formation in TAZ-deficient kidneys is not due to changes in the expression of these cystic disease genes. Polycystin-1 and -2, proteins encoded by ADPKD genes *PKD1* and *PKD2*, respectively, are membrane glycoproteins that can associate with each other to form a complex in the primary cilium of renal epithelial cells (2, 10, 19). The polycystin complex is implicated in cell cycle regulation, intracellular calcium regulation, and maintenance of cellular polarity (2, 10, 19). Polyductin/fibrocystin, the protein encoded by *PKHD1*, is also a large transmembrane protein. Considering the possible interaction of TAZ with membrane-associated PDZ domain-containing proteins, it may still be possible that TAZ and the cystic disease proteins share a common pathway

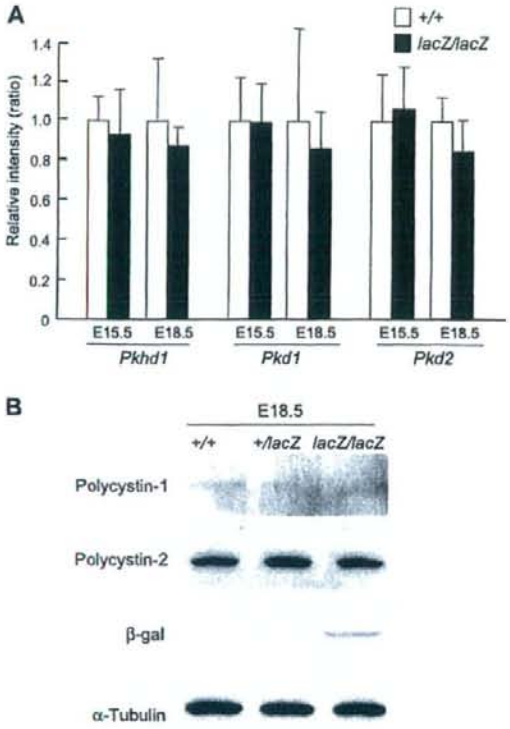

Fig. 8. Real-time RT-PCR analysis and Western blotting of cystic disease genes and proteins. *A*: real-time RT-PCR. Total RNA samples were prepared from *embryonic day 15.5* and *18.5* wild-type (*+/+*) and homozygous (*lacZ/lacZ*) kidneys. The abundance of transcripts for *Pkd1*, *Pkd2*, and *Pkhd1* was measured relative to the internal control *Gapdh*. Error bars indicate SDs of the mean ($n = 5$). For all threes genes at both stages, the expression in homozygous mutant kidneys is not statistically different from wild-type kidney ($P > 0.05$). *B*: Western blotting for polycystin-1 and polycystin-2. Protein levels of polycystin-1 and -2 are not different among wild-type, $Taz^{+/lacZ}$, and $Taz^{lacZ/lacZ}$ kidneys at *embryonic day 18.5*. Blotting for β-galactosidase shows intensities corresponding to the copy number of the *lacZ* gene. Blotting for α-tubulin serves as an internal control.

involved in normal epithelial function and structural integrity. However, taken together with the pathological differences from human PKD, distinct mechanisms may be involved in the renal phenotype of TAZ-deficient mice.

Recently, Hossain et al. (16) also reported the development of cystic kidney disease in TAZ/Wwtr1-deficient mice. Their study suggested that the loss of renal cilia integrity and down-regulation of several genes, including *Pkhd1*, might be associated with the development of renal cysts in TAZ-deficient mice. Independently, Tian et al. (35) have reported that polycystin-2 is overexpressed in adult TAZ-deficient kidneys as a result of decreased ubiquitin-mediated degradation. In the present study, no changes in fibrocystin or polycystin-2 expression are observed in TAZ-deficient kidneys during the prenatal stage, when cyst formation starts. Abnormalities in fibrocystin and polycystin-2 may be involved in later stages of disease progression rather than initial cystogenesis.

Comparison of the renal phenotype of TAZ-deficient mice with human nephrogenic diabetes insipidus. A major difference between the renal phenotype of TAZ-deficient mice and human PKD is the presence of severely dilated calyces and massive polyuria. Although humans with ADPKD and ARPKD may have urinary concentration defects (6, 21), severe polyuria and hydronephrosis are not typical clinical features. TAZ-deficient mice have normal daily excretion of sodium and potassium, indicating that tubular electrolyte reabsorption is well preserved. The relatively low urine osmolality compared with wild-type together with impaired response to exogenous vasopressin are characteristic of nephrogenic diabetes insipidus. Hydronephrosis may be secondary to polyuria, as seen in congenital progressive hydronephrosis (*cph*) mutant mice (22). Thus the renal phenotype of TAZ-deficient mice is characterized by two distinct pathophysiological processes, cyst formation and urinary concentration defects.

Nephrogenic diabetes insipidus is caused by the inability of the renal collecting ducts to reabsorb water in response to vasopressin. About 90% of affected patients have mutations in the *AVPR2* gene, whereas the remaining 10% of patients are caused by *AQP2* gene mutations (28). However, TAZ-knockout kidneys do not show major abnormalities in the levels of expression of *Avpr2*, *Aqp2*, and *Aqp3*. In addition, the apical-basolateral polarity of aquaporin-2 and aquaporin-3 is preserved in both cystic and noncystic collecting ducts at embryonic and postnatal stages. These findings suggest that the polyuria and hydronephrosis in TAZ-deficient mice do not arise from major defects in the expression or localization of the V_2 vasopressin receptor, aquaporin-2, or aquaporin-3. Elucidation of the mechanism underlying the concentration defects in TAZ-deficient kidney may reveal novel pathways regulating renal water transport.

Possible requirement of TAZ for normal kidney development. The kidney develops through reciprocal interactions between the metanephric mesenchyme and the ureteric bud epithelium during embryogenesis (8, 36, 40). The ureteric bud grows into the metanephric mesenchyme and branches to form the collecting duct system while the mesenchyme adjacent to the tips of the ureteric bud is induced to condense and undergo a mesenchymal-to-epithelial transition. The resultant renal vesicle further differentiates into comma- and then S-shaped bodies. Morphogenesis and patterning of the epithelial structures lead to the formation and functional maturation of nephron segments including the glomerulus, the proximal tubule, the loop of Henle, and the distal tubule. Recent advances in gene targeting experiments have greatly contributed to the understanding of molecular mechanisms underlying the early "inductive" phase of kidney development. However, it remains largely unknown how each nephron segment is specified and functionally matures during the late phase of kidney development.

In situ hybridization and β-galactosidase staining demonstrated that *Taz* is diffusely expressed throughout the kidney. *Taz* expression is most intense in the nephrogenic zone during kidney development and is found in both mesenchymal and epithelial cells. *Taz* is not restricted to a specific segment of the nephron. Capillary endothelial cells also express *Taz*. *LacZ* expression is relatively scant and scattered compared with the pattern of in situ hybridization. This difference may be caused

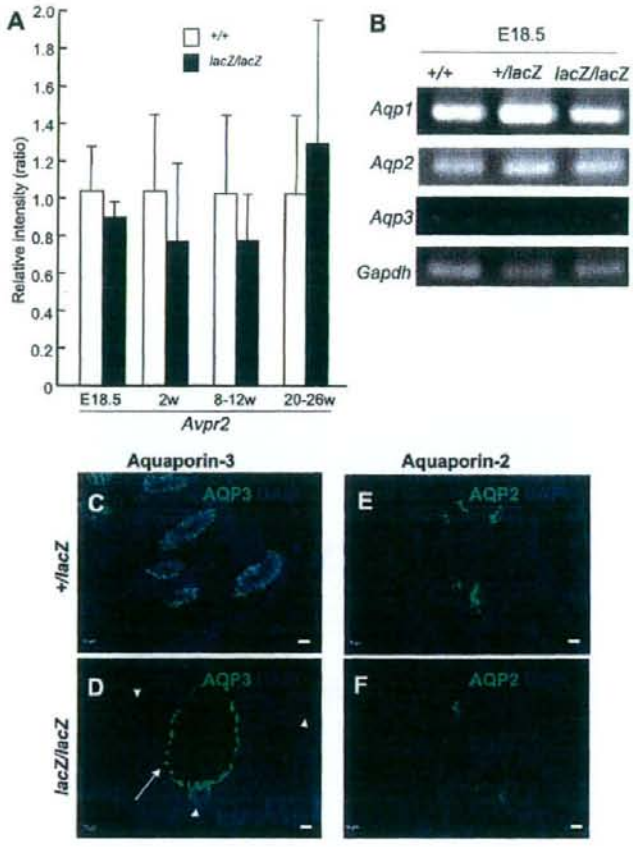

Fig. 9. Expression of genes involved in water transport. *A*: real-time RT-PCR. Total RNA samples were prepared from *embryonic day 18.5* and 2-wk-old wild-type (*+/+*) and homozygous (*lacZ/lacZ*) kidneys. The abundance of transcripts for *Avpr2* was measured relative to the internal control *Gapdh*. Error bars indicate SDs of the mean; $n = 5$ (*+/+*) and 5 (*lacZ/lacZ*) at *embryonic day 18.5*; $n = 4$ (*+/+*) and 3 (*lacZ/lacZ*) at 2 wk; $n = 8$ (*+/+*) and 6 (*lacZ/lacZ*) at 8–12 wk; $n = 4$ (*+/+*) and 4 (*lacZ/lacZ*) at 20–26 wk. No statistically significant difference is detected in the expression of *Avpr2* between *+/+* and *lacZ/lacZ* kidneys ($P > 0.05$). *B*: RT-PCR analysis of *Aquaporin-1*, *-2*, and *-3* expression. Total RNA samples were prepared from *embryonic day 18.5* wild-type (*+/+*), heterozygous (*+/lacZ*), and homozygous (*lacZ/lacZ*) kidneys. The levels of *Aquaporin-1*, *-2*, and *-3* transcripts are not different among wild-type, heterozygous, and homozygous kidneys. RT-PCR for *Gapdh* served as an internal control. *C–F*: immunofluorescence staining of aquaporins. Sections were stained for aquaporin-3 (*C* and *D*) or aquaporin-2 (*E* and *F*) in $Taz^{+/lacZ}$ (*C* and *E*) and $Taz^{lacZ/lacZ}$ (*D* and *F*) kidneys at *embryonic day 18.5*. All sections were costained with 4′,6-diamidine-2-phenylindole. Aquaporin-3 is localized in the basolateral membrane of epithelial cells in some cysts (arrow) as well as in noncystic tubules (arrowheads) in $Taz^{lacZ/lacZ}$ kidneys. Aquaporin-2 is also expressed similarly in collecting ducts in heterozygous and homozygous kidneys. Scale bars indicate 10 μm.

by deletion or disruption of critical enhancer element(s) during the generation of the targeted mutation.

In TAZ-deficient kidneys, most, but not all, of the cyst epithelium is *lacZ*-negative. In contrast, stromal cells, especially in the nephrogenic zone, show strong *lacZ* expression in TAZ-deficient kidneys. This finding indicates that TAZ may be crucial for gene expression in stromal cells supporting normal nephric development.

Pulmonary emphysematous changes in TAZ-deficient mice. In addition to renal cyst formation, TAZ-deficient mice demonstrate severely enlarged air spaces in the lung. This finding is morphologically reminiscent of human pulmonary emphysema, whose genetic pathogenesis is poorly understood. Only a congenital form of emphysema is known to be caused by a deficiency of α-antitrypsin, but its expression was not affected in TAZ-deficient mice (our unpublished data).

Pulmonary emphysema, as a manifestation of COPD, is regarded as a multifactorial disorder triggered by environmental factors such as cigarette smoking and pollutants. Although genetic factors involved in protease/antiprotease balance have been considered as possible determinants of susceptibility to emphysematous changes, the molecular pathogenesis is still unknown. In mice, emphysema-like pulmonary changes can be caused by deficiency in surfactant proteins SP-C or SP-D, possibly through increased activity of matrix metalloproteases (9, 38). Interestingly, TAZ has been reported to be a coactivator for the transcription factor TTF-1/Nkx2.1 and upregulates the expression of SP-C in respiratory epithelial cells (5). However, SP-C expression was not apparently affected in TAZ-deficient lungs (unpublished observations), so different mechanisms may generate the emphysematous changes in TAZ-deficient lungs.

The coexistence of renal and pulmonary abnormalities observed in TAZ-deficient mice has not been described before. However, there are similarities in the embryonic development of the kidney and lung. Both involve common processes, e.g., branching morphogenesis and common signaling pathways such as sonic hedgehog, fibroblast growth factor, and bone morphogenetic protein (17, 41). These similarities raise the possibility that TAZ may be an effector in a common pathway that is involved in both lung and kidney development. Although the apical-basolateral polarity of epithelial cells in collecting ducts is not impaired in TAZ-deficient kidneys, further examination of the processes of epithelial tubule formation in TAZ-deficient kidneys and lungs may reveal a

common mechanism for organogenesis and pathogenesis of human diseases.

ACKNOWLEDGMENTS

We thank Dr. Mark Knepper (National Heart, Lung, and Blood Institute) for the aquaporin-2 antibody.

GRANTS

This work was supported by Grants-in-Aid for Scientific Research from the Ministry of Education, Culture, Sports, Science, and Technology, Japan, Grants-in-Aid for Scientific Research from the Ministry of Health, Labour, and Welfare of Japan, a Research Grant from Uehara Memorial Foundation, the University of Texas Southwestern O'Brien Kidney Research Core Center (National Institute of Diabetes and Digestive and Kidney Diseases Grant P30DK-079328), and a Basil O'Connor Research Grant from the March of Dimes Birth Defects Foundation.

REFERENCES

1. **Barnes PJ.** New concepts in chronic obstructive pulmonary disease. *Annu Rev Med* 54: 113–129, 2003.
2. **Benezra R.** Polycystins: inhibiting the inhibitors. *Nat Cell Biol* 7: 1064–1065, 2005.
3. **Bisceglia M, Galliani CA, Senger C, Stallone C, Sessa A.** Renal cystic diseases: a review. *Adv Anat Pathol* 13: 26–56, 2006.
4. **Chen Q, Takahashi S, Zhong S, Hosoda C, Zheng HY, Ogushi T, Fujimura T, Ohta N, Tanoue A, Tsujimoto G, Kitamura T.** Function of the lower urinary tract in mice lacking alpha1d-adrenoceptor. *J Urol* 174: 370–374, 2005.
5. **Cui CB, Cooper LF, Yang X, Karsenty G, Aukhil I.** Transcriptional coactivation of bone-specific transcription factor Cbfa1 by TAZ. *Mol Cell Biol* 23: 1004–1013, 2003.
6. **D'Angelo A, Mioni G, Ossi E, Lupo A, Valvo E, Maschio G.** Alterations in renal tubular sodium and water transport in polycystic kidney disease. *Clin Nephrol* 3: 99–105, 1975.
7. **Deen PMT.** Mouse models for congenital nephrogenic diabetes insipidus: what can we learn from them? *Nephrol Dial Transplant* 22: 1023–1026, 2007.
8. **Dressler GR.** Tubulogenesis in the developing mammalian kidney. *Trends Cell Biol* 12: 390–395, 2002.
9. **Glasser SW, Detmer EA, Ikegami M, Na CL, Stahlman MT, Whitsett JA.** Pneumonitis and emphysema in sp-C gene targeted mice. *J Biol Chem* 278: 14291–14298, 2003.
10. **Guay-Woodford LM.** Murine models of polycystic kidney disease: molecular and therapeutic insights. *Am J Physiol Renal Physiol* 285: F1034–F1049, 2003.
11. **Gusmano R, Caridi G, Marini M, Perfumo F, Ghiggeri GM, Piaggio G, Ceccherini I, Seri M.** Glomerulocystic kidney disease in a family. *Nephrol Dial Transplant* 17: 813–818, 2002.
12. **Hogg JC.** Pathophysiology of airflow limitation in chronic obstructive pulmonary disease. *Lancet* 364: 709–721, 2004.
13. **Hong JH, Hwang ES, McManus MT, Amsterdam A, Tian Y, Kalmukova R, Mueller E, Benjamin T, Spiegelman BM, Sharp PA, Hopkins N, Yaffe MB.** TAZ, a transcriptional modulator of mesenchymal stem cell differentiation. *Science* 309: 1074–1078, 2005.
14. **Hong JH, Yaffe MB.** TAZ: a β-catenin-like molecule that regulates mesenchymal stem cell differentiation. *Cell Cycle* 5: 176–179, 2006.
15. **Horie S.** ADPKD: molecular characterization and quest for treatment. *Clin Exp Nephrol* 9: 282–291, 2005.
16. **Hossain Z, Ali SM, Ko HL, Xu J, Ng CP, Guo K, Qi Z, Ponniah S, Hong W, Hunziker W.** Glomerulocystic kidney disease in mice with a targeted inactivation of Wwtr1. *Proc Natl Acad Sci USA* 104:1631–1636, 2007.
17. **Hu MC, Rosenblum ND.** Genetic regulation of branching morphogenesis: lessons learned from loss-of-function phenotypes. *Pediatr Res* 54: 433–438, 2003.
18. **Kanai F, Marignani PA, Sarbassova D, Yagi R, Hall RA, Donowitz M, Hisaminato A, Fujiwara T, Ito Y, Cantley LC, Yaffe MB.** TAZ: a novel transcriptional co-activator regulated by interactions with 14-3-3 and PDZ domain proteins. *EMBO J* 19: 6778–6791, 2000.
19. **Li X, Luo Y, Starremans PG, McNamara CA, Pei Y, Zhou J.** Polycystin-1 and polycystin-2 regulate the cell cycle through the helix-loop-helix inhibitor Id2. *Nat Cell Biol* 7: 1102–1112, 2005.
20. **Lu W, Peissel B, Babakhanlou H, Pavlova A, Geng L, Fan X, Larson C, Brent G, Zhou J.** Perinatal lethality with kidney and pancreas defects in mice with a targetted Pkd1 mutation. *Nat Genet* 17: 179–181, 1997.
21. **Martinez-Maldonado M, Yium JJ, Eknoyan G, Suki WN.** Adult polycystic kidney disease: studies of the defect in urine concentration. *Kidney Int* 2: 107–113, 1972.
22. **McDill BW, Li SZ, Kovach PA, Ding L, Chen F.** Congenital progressive hydronephrosis (cph) is caused by an S256L mutation in aquaporin-2 that affects its phosphorylation and apical membrane accumulation. *Proc Natl Acad Sci USA* 103: 6952–6957, 2006.
23. **Mochizuki T, Wu G, Hayashi T, Xenophontos SL, Veldhuisen B, Saris JJ, Reynolds DM, Cai Y, Gabow PA, Pierides A, Kimberling WJ, Breuning MH, Deltas CC, Peters DJ, Somlo S.** PKD2, a gene for polycystic kidney disease that encodes an integral membrane protein. *Science* 272: 1339–1342, 1996.
24. **Murakami M, Nakagawa M, Olson EN, Nakagawa O.** A WW domain protein TAZ is a critical coactivator for TBX5, a transcription factor implicated in Holt-Oram syndrome. *Proc Natl Acad Sci USA* 102: 18034–18039, 2005.
25. **Murakami M, Tominaga J, Makita R, Uchijima Y, Kurihara Y, Nakagawa O, Asano T, Kurihara H.** Transcriptional activity of Pax3 is co-activated by TAZ. *Biochem Biophys Res Commun* 339: 533–539, 2006.
26. **Nagy A, Gertsenstein M, Vintersten K, Behringer R.** *Manipulating the Mouse Embryo: A Laboratory Manual* (3rd ed.). Cold Spring Harbor, NY: Cold Spring Harbor Laboratory, 2003.
27. **Nakagawa O, Nakagawa M, Richardson JA, Olson EN, Srivastava D.** HRT1, HRT2, and HRT3: a new subclass of bHLH transcription factors marking specific cardiac, somitic, and pharyngeal arch segments. *Dev Biol* 216: 72–84, 1999.
28. **Nielsen S, Frøkiær J, Marples D, Kwon TH, Agre P, Knepper MA.** Aquaporins in the kidney: from molecules to medicine. *Physiol Rev* 82: 205–244, 2002.
29. **Onuchic LF, Furu L, Nagasawa Y, Hou X, Eggermann T, Ren Z, Bergmann C, Senderek J, Esquivel E, Zeltner R, Rudnik-Schoneborn S, Mrug M, Sweeney W, Avner ED, Zerres K, Guay-Woodford LM, Somlo S, Germino GG.** PKHD1, the polycystic kidney and hepatic disease 1 gene, encodes a novel large protein containing multiple immunoglobulin-like plexin-transcription-factor domains and parallel beta-helix 1 repeats. *Am J Hum Genet* 70: 1305–1317, 2002.
30. **Park KS, Whitsett JA, Di Palma T, Hong JH, Yaffe MB, Zannini M.** TAZ interacts with TTF-1 and regulates expression of surfactant protein-C. *J Biol Chem* 279: 17384–17390, 2004.
31. **Shao X, Johnson JE, Richardson JA, Hiesberger T, Igarashi P.** A minimal Ksp-cadherin promoter linked to a green fluorescent protein reporter gene exhibits tissue-specific expression in the developing kidney and genitourinary tract. *J Am Soc Nephrol* 13: 1824–1836, 2002.
32. **The European Polycystic Kidney Disease Consortium.** The polycystic kidney disease 1 gene encodes a 14 kb transcript and lies within a duplicated region on chromosome 16. *Cell* 77: 881–894, 1994.
33. **The International Polycystic Kidney Disease Consortium.** Polycystic kidney disease: the complete structure of the PKD1 gene and its protein. *Cell* 81: 289–298, 1995.
34. **Thurlbeck WM.** Measurement of pulmonary emphysema. *Am Rev Respir Dis* 95: 752–764, 1967.
35. **Tian Y, Kolb R, Hong JH, Carroll J, Li D, You J, Bronson R, Yaffe MB, Zhou J, Benjamin T.** TAZ promotes PC2 degradation through a $SCF^{\beta\text{-}Trcp}$ E3 ligase complex. *Mol Cell Biol* 27: 6383–6395, 2007.
36. **Vainio S, Lin Y.** Coordinating early kidney development: lessons from gene targeting. *Nat Rev Genet* 3: 533–543, 2002.
37. **Ward CJ, Hogan MC, Rossetti S, Walker D, Sneddon T, Wang X, Kubly V, Cunningham JM, Bacallao R, Ishibashi M, Milliner DS, Torres VE, Harris PC.** The gene mutated in autosomal recessive polycystic kidney disease encodes a large, receptor-like protein. *Nat Genet* 30: 259–269, 2002.
38. **Wert SE, Yoshida M, LeVine AM, Ikegami M, Jones T, Ross GF, Fisher JH, Korfhagen TR, Whitsett JA.** Increased metalloproteinase activity, oxidant production, and emphysema in surfactant protein D gene-inactivated mice. *Proc Natl Acad Sci USA* 97: 5972–5977, 2000.
39. **Witzgall R.** The proximal tubule phenotype and its disruption in acute renal failure and polycystic kidney disease. *Exp Nephrol* 7: 15–19, 1999.
40. **Yu J, McMahon AP, Valerius MT.** Recent genetic studies of mouse kidney development. *Curr Opin Genet Dev* 14: 550–557, 2004.
41. **Zegers MM, O'Brien LE, Yu W, Datta A, Mostov KE.** Epithelial polarity and tubulogenesis in vitro. *Trends Cell Biol* 13: 169–176, 2003.

INTERNAL MEDICINE

□ CASE REPORT □

Non-Infectious Bronchiolitis as an Early Pulmonary Complication of Hematopoietic Stem Cell Transplantation

Hidenori Kage[1], Tadashi Kohyama[1], Hiroshi Kitagawa[1], Daiya Takai[2], Yoshinobu Kanda[3], Nobuya Ohishi[1] and Takahide Nagase[1]

Abstract

Pulmonary complications occur in up to 60% of patients after hematopoietic stem cell transplantation (HSCT), causing significant morbidity and mortality. Among them, non-infectious bronchiolitis is considered a late complication in the form of bronchiolitis obliterans. We report a patient who developed non-infectious bronchiolitis within four weeks after undergoing HSCT for biphenotypic leukemia. Chest CT revealed centrilobular nodules that were reminiscent of diffuse panbronchiolitis, and lymphocytic bronchiolitis was confirmed by biopsy. Infection and bronchiolitis obliterans were ruled out, and the bronchiolitis resolved when leukemia relapsed. This case suggests that bronchiolitis may be another early, non-infectious pulmonary complication of HSCT.

Key words: bronchiolitis, hematopoietic stem cell transplantation, diffuse panbronchiolitis

(DOI: 10.2169/internalmedicine.47.0456)

Introduction

Hematopoietic stem cell transplantation (HSCT) is used to treat hematological, neoplastic, autoimmune, and genetic diseases, often providing prolonged survival. However, complications are common in the lung; they occur in up to 60% of patients, and account for more than 30% of all transplantation-related deaths (1). They are classified as infectious or non-infectious, and a higher proportion of non-infectious complications have accounted for morbidity and mortality in recent years because the incidence of infection has diminished with effective prophylaxis. Several non-infectious pulmonary complications have been recognized: pulmonary edema, engraftment syndrome, diffuse alveolar hemorrhage, idiopathic pneumonia syndrome, veno-occlusive disease, organizing pneumonia, and bronchiolitis obliterans (BO) (1, 2). BO usually develops after the first 100 days post-transplant, and bronchiolitis other than BO have not been recognized as an early, non-infectious complication of HSCT. Here, we report a case of non-infectious bronchiolitis distinct from BO that developed within the first month of HSCT.

Case Report

A 19-year-old man developed dyspnea, impaired hemostasis, and arthralgia of the lower limbs. Blood tests revealed WBC 198,000/μL, Hb 5.1 g/dL, Plt 15,000/μL. He was admitted for suspected leukemia. Bone marrow aspiration revealed that 67% of nucleated cells were blasts, which were positive for CD10, CD13, CD14, CD19, CD20, CD22, CD33, CD34, HLA-DR, and myeloperoxidase, and a diagnosis of acute biphenotypic leukemia of B cell and myeloid lineage was made according to the European Group of Immunological Classification of Leukemias criteria (3). Two courses of chemotherapy consisting of 170 mg/day of cytarabine on days 1-7 and 20 mg/day of idarubicin on days 5-7 resulted in induction failure, as did two courses of high-dose cytarabine of 6,800 mg/day on days 1-4 and 12 mg/day of mitoxantrone on days 1-2. On-disease allogeneic peripheral blood stem cell transplantation from a completely HLA-

[1]Department of Respiratory Medicine, The University of Tokyo, Tokyo, [2]Department of Clinical Laboratory, The University of Tokyo, Tokyo and [3]Division of Hematology, Omiya Medical Center, Jichi Medical School, Omiya
Received for publication July 17, 2007; Accepted for publication September 21, 2007
Correspondence to Dr. Hidenori Kage, kageh-tky@umin.ac.jp

DOI: 10.2169/internalmedicine.47.0456

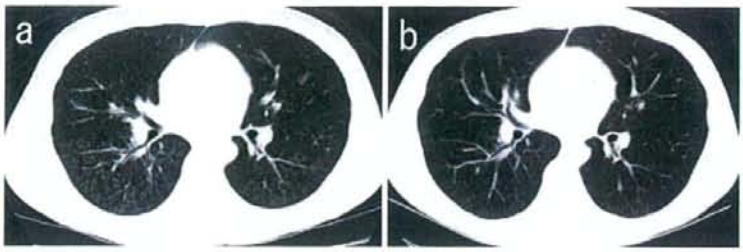

Figure 1. **a) Chest CT on day 25 after transplantation, showing small, diffuse, centrilobular nodules, consistent with bronchiolitis. b) Chest CT on day 46, showing that the nodules have regressed.**

matched sibling [HLA-A (31, 33), B (51, 58), and DR (0301, 0802)] was performed. Pre-transplant paranasal sinus radiograph, chest CT, and spirometry were normal. The conditioning regimen was 2 Gy of total body irradiation twice a day on days -6 to -4 for a total of 12 Gy, and 3,500 mg/day of cyclophosphamide on days -3 and -2. As prophylaxis against graft-versus-host disease (GVHD), he was given 170 mg/day of cyclosporine starting from day -1, and 17 mg of methotrexate on day1 and 12 mg/day on days 3 and 6. Cefepime, vancomycin, micafungin, and acyclovir were given as prophylaxes against infection. CD34-positive peripheral blood stem cells were infused at a dose of 4.4×10^6 cells/kg. Engraftment was confirmed on day 23. On the same day, erythema of the palms and soles were noted, and grade 1 acute GVHD was diagnosed.

A fever of 37.6 degrees, purulent sputum, and dyspnea developed on day 24. On auscultation, lungs were clear. Serum fungal antigens for *Aspergillus*, *Cryptococcus*, and *Candida*, and the cytomegalovirus (CMV) pp65 antigenemia assay were negative. Chest radiograph showed diffuse nodular shadows in both lower lung fields, and sinus X-ray showed fluid in the maxillary sinuses. Bone marrow aspiration on day 30 revealed no blasts, confirming remission. Chest CT on day 32 revealed diffuse, bilateral centrilobular nodules with a predominance in the lower lung fields (Fig. 1A), and sinus CT showed fluid and mucosal thickening of the frontal, maxillary, ethmoidal, and sphenoid sinuses, together reminiscent of diffuse panbronchiolitis (DPB). Arterial blood gas showed pH 7.42, PaO_2 75 Torr, and $PaCO_2$ 40 Torr while breathing ambient air. Pulmonary function tests showed declines in FEV_1, from 4.1 L to 2.4 L, and in FEV_1%, from 91% to 67%, and an increase in $\dot{V}50/\dot{V}25$, from 1.9 to 4.3, indicating significant airflow obstruction. %VC, %RV, %TLC, and RV/TLC all declined from 99% to 90%, from 132% to 80%, from 95% to 78%, and from 29% to 21%, respectively. Diffusing capacity was unchanged. Analysis of broncho-alveolar lavage fluid (BALF) showed total cell counts of 58×10^5 cells/ml with differential cell counts of 25% macrophages, 50% lymphocytes, and 25% eosinophils. Of the lymphocytes, 95% were CD3-positive T cells, and the CD4/8 ratio was 0.70. The peripheral blood white blood cell count was 6,500/μl, and the leukocyte differentials showed 42% neutrophils, 31% eosinophils, 4% basophils, 18% monocytes, and 5% lymphocytes. Bacterial, mycobacterial, and fungal cultures of the BALF were negative, as were the polymerase chain reaction assays for *Aspergillus*, *Pneumocystis jiroveci*, CMV, respiratory syncytial virus, parainfluenza virus, and adenovirus, ruling out infection. Histological examination of trans-bronchial lung biopsy showed lymphocytic bronchitis and bronchiolitis with involvement of adjacent alveoli (Fig. 2). Very few eosinophils were seen. The infiltrating lymphocytes were CD8-positive T cells. The histological findings were not indicative of any infection or bronchiolitis obliterans.

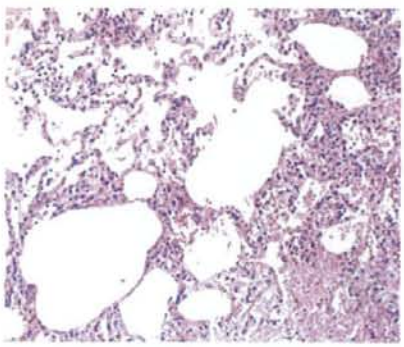

Figure 2. **Transbronchial biopsy (Hematoxylin and Eosin staining, ×100) shows lymphocytic bronchiolitis with involvement of the adjacent alveoli.**

Chest CT on day 46 showed that the lesions had regressed without any treatment (Fig. 1B). On the same day, leukemia cells were found in the peripheral blood, indicating disease relapse, and resolution of GVHD was also observed. The patient died of leukemia on day 64.

Discussion

We have described a case of non-infectious lymphocytic bronchiolitis that developed within a month of HSCT. Chest CT showed centrilobular nodules, pulmonary function tests showed airflow limitation without a decrease in diffusing capacity, and biopsy confirmed the presence of lymphocytic bronchiolitis. There was no evidence of infection, and the clinical picture was quite different from any of the well-

described non-infectious pulmonary complications of HSCT: pulmonary edema, peri-engraftment respiratory distress syndrome, diffuse alveolar hemorrhage, idiopathic pneumonia syndrome, veno-occlusive disease, organizing pneumonia, or BO (1, 2). The present case suggests that bronchiolitis may represent another early, non-infectious pulmonary complication of HSCT.

We do not consider the present case to be BO for three reasons. First, BO usually develops after the first 100 days after transplantation (4). Second, the typical CT findings of BO are air trapping, small airway thickening, or bronchiectasis, not centrilobular nodules (4). Third, biopsy findings did not show any fibrosis or eosinophilic scarring of the bronchioles resulting in narrowing of the lumen, suggestive of BO (5). It has been reported that airflow obstruction develops in the early stages after HSCT without any finding suggestive of BO (6). Therefore, it is possible that some cases of BO are sequelae of early bronchiolitis. Early bronchiolitis may have previously gone mostly unnoticed because of its mild clinical course.

The significance of an increase of eosinophils in the BAL fluid is unclear because only a few eosinophils were seen in biopsy specimens. This discrepancy is sometimes seen in diffuse lung diseases; however, what it indicates is not known. We consider that eosinophils had less of a role compared to lymphocytes based on the histological findings.

The chest CT finding of diffuse, centrilobular nodules with a lower lobe predominance together with clinical syndromes of purulent sputum, dyspnea, sinusitis, and airflow limitation was reminiscent of diffuse panbronchiolitis (DPB), a disease with chronic inflammation of the respiratory bronchioles most often seen in East Asians (7). However, it is clear he did not have DPB because there was no airflow obstruction and chest CT was normal before transplantation. It is possible that bronchiolitis and sinusitis share a common etiology, causing a sinobronchial syndrome, but infection was never ruled out. Therefore, the significance of sinusitis is unclear.

As a complication of HSCT, there have previously been several pathological descriptions of airway disease other than BO. Beschorner et al examined autopsy material from 59 patients with a mean survival of 48 days after receiving bone marrow transplants, and found that 15 had lymphocytic bronchitis (8). Yousem reviewed lung biopsy specimens and described lymphocytic bronchitis or bronchiolitis, distinct from BO, with cellular interstitial pneumonia as one of the manifestations of pulmonary GVHD (9). There have also been case reports of lymphocytic pneumonitis, but not bronchiolitis (10, 11). To our knowledge, this is the first clinical report on early, non-infectious, non-BO bronchiolitis complicating HSCT.

The pathogenesis of the well-recognized, early, non-infectious pulmonary complications have not yet been fully elucidated, but proposed mechanisms include conditioning-related toxicities, immune-mediated injury, and occult infection (1). The pathogenesis of non-infectious bronchiolitis remains obscure. Beschorner et al reported that the development of lymphocytic bronchitis was significantly correlated with the presence of GVHD (8), which is in agreement with the report of Yousem (9) and that using a rat model (12). On the other hand, some have suggested that lymphocytic bronchitis is unrelated to GVHD, using canine models (13). In the present case, because infection was effectively ruled out, and because the bronchiolitis was resolved without any treatment as leukemia relapsed and GVHD subsided, an immune-mediated injury in which the donor lymphocytes attack the recipient airway cells, may be the most plausible explanation.

In conclusion, the present case suggests that bronchiolitis may be considered a distinct form of early non-infectious pulmonary complication of HSCT.

References

1. Kotloff RM, Ahya VN, Crawford SW. Pulmonary complications of solid organ and hematopoietic stem cell transplantation. Am J Respir Crit Care Med **170**: 22-48, 2004.
2. Sirithanakul K, Salloum A, Klein JL, Soubani AO. Pulmonary complications following hematopoietic stem cell transplantation: diagnostic approaches. Am J Hematol **80**: 137-146, 2005.
3. Bene MC, Castoldi G, Knapp W, et al. Proposals for the immunological classification of acute leukemias. European Group for the Immunological Characterization of Leukemias (EGIL). Leukemia **9**: 1783-1786, 1995.
4. Filipovich AH, Weisdorf D, Pavletic S, et al. National Institutes of Health consensus development project on criteria for clinical trials in chronic graft-versus-host disease: I. Diagnosis and staging working group report. Biol Blood Marrow Transplant **11**: 945-956, 2005.
5. Shulman HM, Kleiner D, Lee SJ, et al. Histopathologic diagnosis of chronic graft-versus-host disease: National Institutes of Health Consensus Development Project on Criteria for Clinical Trials in Chronic Graft-versus-Host Disease: II. Pathology Working Group Report. Biol Blood Marrow Transplant **12**: 31-47, 2006.
6. Chien JW, Martin PJ, Flowers ME, Nichols WG, Clark JG. Implications of early airflow decline after myeloablative allogeneic stem cell transplantation. Bone Marrow Transplant **33**: 759-764, 2004.
7. Azuma A, Kudoh S. Diffuse panbronchiolitis in East Asia. Respirology **11**: 249-261, 2006.
8. Beschorner WE, Saral R, G.M. Hutchins GM, Tutschka PJ, Santos GW. Lymphocytic bronchitis associated with graft-versus-host disease in recipients of bone-marrow transplants. N Engl J Med **299**: 1030-1036, 1978.
9. Yousem SA. The histological spectrum of pulmonary graft-versus-host disease in bone marrow transplant recipients. Hum Pathol **26**: 668-675, 1995.
10. Atkinson K, Turner J, Biggs JC, Dodds A, Concannon S. An acute pulmonary syndrome possibly representing acute graft-versus-host disease involving the lung interstitium. Bone Marrow Transplant **8**: 231-234, 1991.
11. Bolanos-Meade J, Ioffe O, Hey JC, Vogelsang GB, Akpek G. Lymphocytic pneumonitis as the manifestation of acute graft-versus-host disease of the lung. Am J Hematol **79**: 132-135, 2005.

DOI: 10.2169/internalmedicine.47.0456

12. Workman DL, Clancy J Jr. Interstitial pneumonitis and lymphocytic bronchiolitis/bronchitis as a direct result of acute lethal graft-versus-host disease duplicate the histopathology of lung allograft rejection. Transplantation **58**: 207-213, 1994.

13. O'Brien KD, Hackman RC, Sale GE, et al. Lymphocytic bronchitis unrelated to acute graft-versus-host disease in canine marrow graft recipients. Transplantation **37**: 233-238, 1984.

ARTICLE IN PRESS
+ MODEL
Respiratory Medicine (2008) xx, 1–8

available at www.sciencedirect.com

ScienceDirect

journal homepage: www.elsevier.com/locate/rmed

Clarithromycin inhibits fibroblast migration

Tadashi Kohyama [a,*], Yasuhiro Yamauchi [a], Hajime Takizawa [b], Susumu Itakura [a], Sumiko Kamitani [a], Jun Kato [a], Takahide Nagase [a]

[a] *Department of Respiratory Medicine, The University of Tokyo, Graduate School of Medicine, 7-3-1 Hongo Bunkyo-ku, Tokyo 113-8655, Japan*
[b] *Fourth Department of Internal Medicine, Teikyo University, School of Medicine, Kawasaki, Japan*

Received 13 March 2008; accepted 30 June 2008

KEYWORDS
Fibroblast;
Macrolide;
Clarithromycin;
Migration

Summary
The aim of the current study was to investigate the effect of 14-membered ring macrolide clarithromycin (CAM) on migration induced by human plasma fibronectin (HFn) or on contraction of human fetal lung fibroblasts (HFL-1).
Methods and results: Using the blindwell chamber technique, CAM (10^{-5} M) inhibited the migration of HFL-1 60.2 ± 4.0% ($p < 0.05$). Other antibiotics, such as ampicillin, minocycline or azithromycin had no effects on HFL-1 migration. The effect of CAM was concentration dependent. HFL-1 migration, stimulated by TXA_2 analog was also inhibited by CAM. Clarithromycin had no effect on HFL-1 mediated gel contraction that was another function of fibroblast at the wound area.
Conclusions: Clarithromycin may contribute to the regulation of the wound healing response following injury by inhibiting fibroblast migration. These results could represent the therapeutic benefits of CAM.

Introduction

After tissue injury, fibroblast migration from surrounding peri-wound connective tissue into the site of wound area and fibroblast contraction at wound area plays an important role in repairing process. Under normal circumstances, fibroblasts are quiescent mesenchymal cells. However, in some inflammatory processes, fibroblasts become activated and excess number of their migration would cause replacement of normal parenchymal elements of tissue to fibrosis.[1] These changes can distort normal tissue architectural relationship, can compromise organ function and can cause fibrosis. One of the therapeutic objectives in fibrotic disease is to reduce the local inflammatory response through the reduction of excess migration and contraction of fibroblast.

The macrolide is a group of antibiotics which have unique large macrocyclic lactone ring. Macrolide inhibits bacterial protein biosynthesis by binding to the subunit 50S of the bacterial ribosome. Macrolide is effective against Gram-positive cocci, mycoplasma, mycobacteria, and chlamydia.

* Corresponding author. Tel.: +81 03 3815 5411; fax: +81 03 3815 5954.
E-mail address: koyama-tky@umin.ac.jp (T. Kohyama).

0954-6111/$ - see front matter © 2008 Elsevier Ltd. All rights reserved.
doi:10.1016/j.rmed.2008.06.020

Please cite this article in press as: Kohyama T et al., Clarithromycin inhibits fibroblast migration, Respiratory Medicine (2008), doi:10.1016/j.rmed.2008.06.020

Among them, 14-membered ring macrolides, however, have curious effects on inflammatory processes. Low dose erythromycin therapy improves the survival or lung function of patient with intractable diseases, such as diffuse panbronchiolitis (DPB) which is mostly recognized in Asian and cystic fibrosis which is most common inherited disease in Caucasian.[2,3] According to the data of inhibition of inflammatory cytokine productions,[4–6] changing the Th1/Th2 cytokine ratio[3] and effectiveness in cancer studies,[7–9] macrolide effects might be immunomodulatory activities. In vivo study also shows that macrolide might prevent the lung injury and fibrosis in bleomycin-challenged mouse.[10]

However, the precise mechanism of 14-membered ring macrolide has not been elucidated clearly yet. The current study evaluated the potential effects of CAM on fibroblast-mediated repair responses by using *in vitro* models of tissue remodeling. Our findings, therefore, support the notion that CAM may play a role in the remedy of remodeling of the lung.

Materials and methods

Materials

Clarithromycin was generously provided by Taisho Pharmaceutical Co. (Tokyo, Japan). Ampicillin (ABPC), minocycline (MINO) and azithromycin (AZM) were purchased from SIGMA (St. Louis, MO). KT5720 was purchased from Calbiochem (San Diego, CA). Ampicillin (10^{-2} M), MINO (2×10^{-2} M) was dissolved into dH_2O, CAM (5×10^{-3} M) and AZM(10^{-3} M) were dissolved into 100% ethanol and KT5720 was dissolved into dimethylsulfoxide (DMSO) at 10^{-2} M for stock reagents.

According to the reports of previous experiments,[11,5,4,12] we chose the concentration of each drugs as follows: MINO (10^{-6} M); ABPC (10^{-5} M); CAM (10^{-5} M); AZM (10^{-5} M). Those concentrations were around the clinical plasma levels achieved pharmacologically after using standard dosage.

Tissue culture supplements and media were purchased from GIBCO (Life Technologies, Grand Island, NY). Fetal calf serum (FCS) was purchased from Biofluid (Rockville, MD). Human fetal lung fibroblasts (HFL-1) were obtained from the American Type Culture Collection (Rockville, MD). A second strain of human fetal lung fibroblasts (WI-38) was purchased from Health Science Research Resources Bank (Osaka, Japan). The cells were cultured in 100 mm tissue culture dishes (FALCON; Becton–Dickinson Labware, Lincoln Park, NJ) in Dulbecco's modified Eagle medium (DMEM, Gibco, Grand Island, NY), supplemented with 10% FCS, 50 U/ml penicillin G sodium and 50 μg/ml streptomycin sulfate (penicillin–streptomycin, GIBCO) in a humidified atmosphere at 37 °C and 5% CO_2. The fibroblasts were routinely passaged every 4 or 5 days and cells were used between passage 13 and 21 in all experiments. Subconfluent fibroblasts were removed from the dishes by treatment with 0.05% trypsin in 0.53 mM ethylenediaminetetraacetic acid and stop the reaction by soybean trypsin inhibitor (GIBCO). After centrifuging to remove the trypsin inhibitor, cells were re-suspended in DMEM without serum.

Cell toxicity examination

Preliminary, MTT assay was performed to test the toxicity of reagents and diluents. Briefly, after being cultured for 6 h with each reagent in 96 well culture plate, the medium were discarded and 100 μl MTT solution (200 μg/ml in DMEM) per well was added. After another 4 h incubation, MTT solution were discarded and 100 μl of DMEM per well was added to melt formazan crystal. The OD values were read at 630 nm wavelength.

Fibroblast migration

HFL-1 and WI-38 migrations were assessed by the Boyden blindwell chamber system[13] using 48-well chambers (Nucleopore, Cabin John, MD). The chemoattractant fibronectin was placed in the bottom chamber. The upper and lower portions of the chamber were separated by the 8 μm pore filter (Nucleopore, Pleasanton, CA) coated with 0.1% gelatin (Bio Rad, Hercules, CA). The top manifold was placed and human fetal lung fibroblasts (1.0×10^6 ml in DMEM without serum) were loaded into the upper wells of the chamber with the desired concentration of CAM or

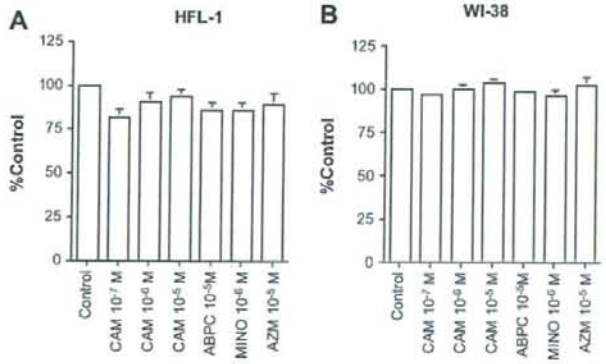

Figure 1 MTT assay. Vertical axis, expressed as percentage of control. Horizontal axis: conditions. (A) HFL-1, (B) WI-38. Data shown are means + SEM for three separate experiments. Each conditions for MTT assay in triplicate.

Please cite this article in press as: Kohyama T et al., Clarithromycin inhibits fibroblast migration, Respiratory Medicine (2008), doi:10.1016/j.rmed.2008.06.020

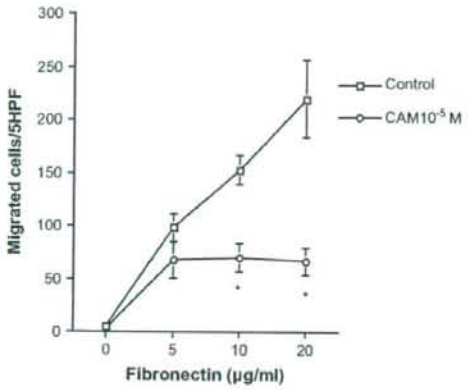

Figure 2 Inhibition of fibroblast migration by CAM. Migration of HFL-1 fibroblasts was measured with blindwell assay system using human fibronectin with or without the CAM (10^{-5} M). Vertical axis, fibroblast migration expressed as number of cells migrated per 5 high-power fields; horizontal axis: concentration of fibronectin. Data shown are means ± SEM for representative data from three separate experiments. Each experiments for migration in triplicate. ($^*p < 0.05$).

other additives. The chamber was then incubated at 37 °C in a moist, 5% CO_2 atmosphere. Except the time course experiment chambers were incubated for 6 h, after which the cells on the top of the filter were removed by scraping. The filter was then fixed, stained with Diff Quik stain (International reagents CORP, Kobe, Japan), and mounted on a glass microscope slide. Migration was assessed by counting the number of cells in 5 high-power fields using a light microscope. Triplicate wells were prepared in each experiment for every condition. Replica experiments were performed with separate cultures of cells on separate occasions.

Collagen gel contraction assay

To test the CAM effect on contractility of fibroblast, another function of fibroblast, fibroblast-mediated gel contraction was measured according to a method developed by Bell and coworkers.[14] Collagen gels were prepared as described previously.[15] Briefly, Type I collagen that was extracted from rat tail,[16] distilled water, 4 × DMEM and fibroblast suspensions were mixed by pipetting so that the final mixture resulted in 0.75 mg/ml of collagen, 3×10^5 fibroblasts/ml gel and a physiologic ionic strength of 1 × DMEM. A 500 μl portion of the gel solution was then cast into each well of a 24-well tissue culture plate (FALCON). After gelation, the gels were released into 60 mm tissue culture dishes (FALCON) containing 5 ml of DMEM with designed concentration of CAM. The floating gels were cultured for up to 5 days, and the ability of the fibroblasts to contract the gels was determined by quantifying the area of the gels daily using an image analyzer (ATTO, Tokyo, Japan).

Statistical analysis

Samples with multiple comparisons were analyzed for significance using analysis of variance (ANOVA). Pair-wise comparisons were analyzed by independent two sample *t*-test where the critical value is adjusted for multiple comparisons by the Tukey test. ($p < 0.05$) Summary data are expressed as mean ± SEM.

Results

MTT assay showed that each concentration of the reagents and diluents using these experiments were not toxic for the fibroblasts (Fig. 1).

The migration was measured by using the blindwell assay system. Fibronectin put in the lower wells directed the

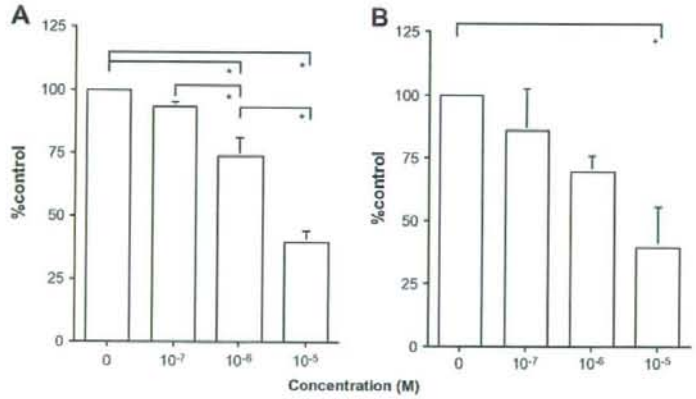

Figure 3 Inhibition of fibroblast migration by CAM: concentration dependence. Fibronectin (20 μg/ml) was used as the chemoattractant. Clarithromycin was added to the fibroblasts at various concentrations immediately before the cells were placed in the top wells of the chemotaxis chamber. (A) HFL-1, (B) WI-38. Vertical axes: fibroblast migration expressed as a percentage of that control. Horizontal axis: CAM concentration. Data shown are means + SEM for triplicate separate experiments, each assayed for chemotactic activity in triplicate. ($^*p < 0.05$).

Please cite this article in press as: Kohyama T et al., Clarithromycin inhibits fibroblast migration, Respiratory Medicine (2008), doi:10.1016/j.rmed.2008.06.020

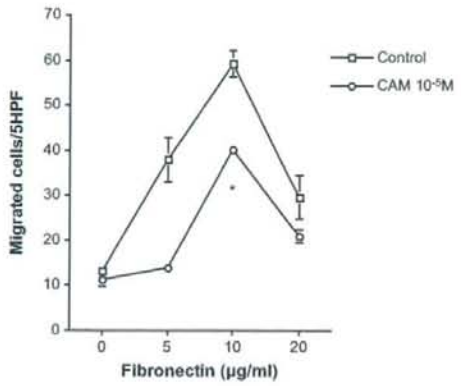

Figure 4 Clarithromycin effect on the chemokinesis of HFL-1. Same concentrations of human fibronectin were placed both above and below the filter. There is no chemoattractant gradient. Vertical axes: fibroblast migration expressed as number of cells migrated per 5 high-power fields; Horizontal axis: fibronectin concentration of both sides. Data shown are means ± SEM for representative data from three separate experiments. Each experiments for migration in triplicate. (*$p < 0.05$).

HFL-1 migration in concentration dependent fashion. Clarithromycin (10^{-5} M) added in the top wells inhibited the HFL-1 migration at 10 and 20 μg/ml of fibronectin (Fig. 2).

Clarithromycin inhibited the fibronectin (20 μg/ml) directed migration in concentration dependent manner. The inhibitory effect reached significant by 10^{-6} M of CAM on HFL-1 (control, 100%; CAM 10^{-6} M, 73.7 ± 7.3%, $p < 0.05$) and by 10^{-5} M of CAM on WI-38 (control, 100%; CAM 10^{-5} M, 46.2 ± 15.5%, $p < 0.05$) (Fig. 3).

To determine if CAM inhibit chemokinesis, same concentrations of human fibronectin were placed both above and below the filter. The meaning of this experiment shows there is no chemoattractant gradient (chemokinesis) even in the presence of increasing concentrations of fibronectin above and below the filter. Clarithromycin also inhibited chemokinesis (at fibronectin 10 μg/ml; control, 59.3 ± 2.9; CAM 10^{-5} M, 40.3 ± 0.9%, $p < 0.05$) (Fig. 4).

In the time course assay, the accumulation of the HFL-1 continued to increase even at the end point we tested (12 h). Clarithromycin (10^{-5} M) inhibited the HFL-1 migration at 6 h (control, 76.0 ± 5.6; CAM, 10^{-5} M 48.0 ± 7.1%, $p < 0.05$) (Fig. 5).

To elucidate the inhibitory effects of CAM on the activated fibroblast as in the inflammatory area, we tested the CAM effect on the fibroblast activated by TXA_2 analog U46619. Clarithromycin (10^{-5} M) significantly inhibited the U46619 (2×10^{-7} nM) activated fibroblasts migration (control = 100%; U46619, 130.3 ± 8.2; U46619 plus CAM 10^{-5} M, 53.1 ± 2.5%, $p < 0.05$) (Fig. 6).

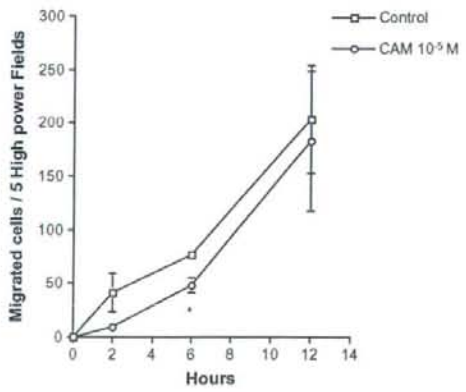

Figure 5 Inhibition of fibroblast migration by CAM: time course. Fibronectin (20 μg/ml) was used as the chemoattractant. Clarithromycin was added to the fibroblasts in the top wells at various concentrations. The chambers were incubated and after varying times, removed for staining and counting. Vertical axis: fibroblast migration expressed as number of cells migrated per 5 high-power fields; horizontal axis: time in hours. Data shown are means ± SEM for representative data from three separate experiments. Each experiment for migration in triplicate (*$p < 0.05$).

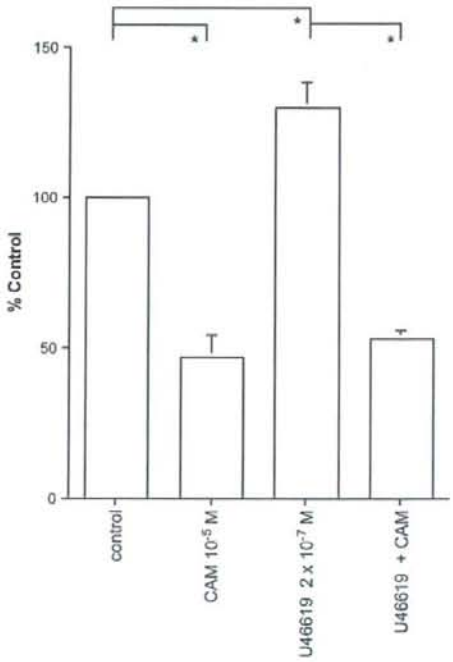

Figure 6 Effect of CAM on stimulatory cells by TXA_2 analog U46619. HFL-1 were pre-incubated with U46619 (2×10^{-7} M) in monolayer culture for 1 h and then harvested for migration. Fibronectin (20 g/ml) was used as chemoattractant. Clarithromycin (10^{-5} M) was added to the fibroblasts in the top wells with 2×10^{-7} M of U46619. Vertical axis, fibroblast migration expressed as percentage of control. Data are means + SEM for triplicate cultures each assayed for migration in triplicate. (*$p < 0.05$).

Please cite this article in press as: Kohyama T et al., Clarithromycin inhibits fibroblast migration, Respiratory Medicine (2008), doi:10.1016/j.rmed.2008.06.020

We have tried to check another antibiotics Ampicillin (ABPC) (10^{-5} M), minocycline (MINO) (10^{-6} M) and azithromycin (AZM) (10^{-5} M) effects on human lung fibroblast migration. Among them CAM but other antibiotics inhibited the migration of HFL-1. (control = 100%; ABPC $90.7 \pm 5.1\%$; MINO, $105.6 \pm 9.7\%$; CAM $45.8 \pm 4.6\%$ $p < 0.05$; AZM $99.5 \pm 15.3\%$) (Fig. 7A). As azithromycin is one of the macrolides, we confirmed its effect with several concentrations. Azithromycin had no effect on HFL-1 migration (Fig. 7B).

Among the fibroblast functions in the wound area, contractility is also important for repair and remodeling process. To elucidate the CAM effect on it, we have used gel contraction assay system. Clarithromycin had no effect on fibroblast contraction in the gel (Fig. 8).

There is no clear mechanism report of CAM effect on fibroblast migrations. Most of the reagents which inhibit the fibroblast migrations are related to the activation of protein kinase A.[17,18] To determine if the inhibition of migration toward fibronectin by CAM is by way of PKA pathway, we assessed the PKA inhibitor KT5720 with CAM. As there is the report which showed that KT5720 block the inhibitory effect of PGD_2 on fibroblast migration,[18] we put the PGD_2 examination as control. KT5720 did not block the inhibitory effect of CAM on HFL-1 migration (Fig. 9).

Discussion

The current study demonstrates that CAM was capable of inhibiting fibroblast migration to human fibronectin. The effects by CAM were concentration dependent. Clarithromycin also inhibited the TXA_2 analog U46619 stimulated migration of HFL-1. Moreover, CAM inhibited both human lung fibroblast chemotaxis and chemokinesis. Clarithromycin had no effect on contractility of fibroblast that is important function for end stage of wound healing.

The accumulation of fibroblasts to the wound site is often a key event in both normal repair and in the development of fibrosis.

In the process of it, fibroblast migration, proliferation and contraction are essential events. Under normal repair process, adequate numbers of fibroblasts migrate to the wound area.

However, an excess accumulation of fibroblasts and excess deposition of extracellular matrix produced by fibroblast results in replacement of the normal tissue parenchyma with fibrotic scar, which results in irreversible distortion of the lung's architecture and compromising organ function.[19,1]

Idiopathic pulmonary fibrosis (IPF) is a chronic, progressive and fetal lung disorder. The mean prognosis after diagnosis is ranging from 3 to 5 years.[20] The treatments employed currently are steroids and cytotoxic agents, however, both of them have not been proven to prolong survival or improve pulmonary function among patients with IPF. The critical phenomenon which related prognosis is ongoing epithelial damage and persistent fibroblastic proliferation.[21]

In this context, the reagent which controls the fibroblast function might be a good medicine.

Clarithromycin, a 14-membered ring macrolide, is known as an antibiotic. Recently we have used this medicine as immunomodulatory drug. This opinion is supported by in vitro and in vivo data. Clarithromycin decreases the production of cytokines,[4–6] changes the Th1/Th2 cytokine ratio[3] and prevents the lung injury and fibrosis in bleomycin-challenged mouse.[10]

These reports will give us hints to explore that clarithromycin might make biological actions on the cells which are important for wound healing or remodeling in the inflammatory milieu.

Our data showed that CAM inhibited fibroblast migration. This is important effect for inhibiting the remodeling.

Fibronectin of plasma is chemotactic for HFL-1 and WI-38.

For the reason mentioned below, we used the fibronectin for chemoattractant of fibroblasts. Fibronectin, one of the extracellular matrixes, is mainly produced by fibroblasts[22] and soluble in plasma and tissues. Fibronectin

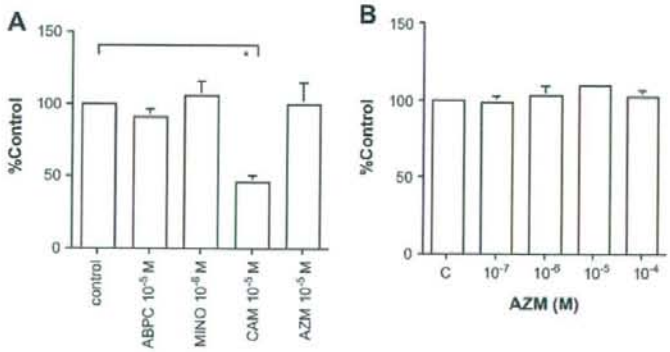

Figure 7 Effects of other antibiotics on fibroblast chemotaxis. HFL-1 migration was performed in the Boyden blind well chamber assay system. (A) Ampicillin (ABPC) (10^{-5} M), minocycline (MINO) (10^{-6} M), CAM (10^{-9} M) and azithromycin (AZM) (10^{-5} M) were added to the top of each well. (B) Several concentration of AZM was tested. Vertical axis, fibroblast migration expressed as percentage of control. Horizontal axis: each condition. Data are means + SEM for triplicate cultures each assayed for migration in triplicate. ($^*p < 0.05$).

Please cite this article in press as: Kohyama T et al., Clarithromycin inhibits fibroblast migration, Respiratory Medicine (2008), doi:10.1016/j.rmed.2008.06.020

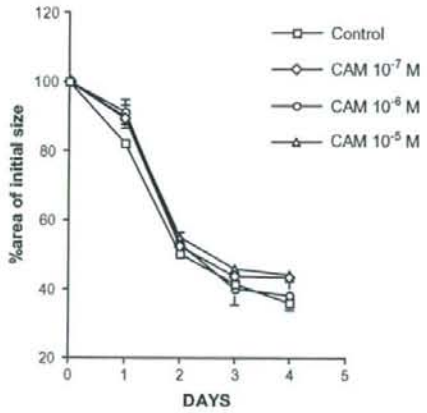

Figure 8 Effect of CAM on collagen gel contraction. HFL-1 was cast into gel and floated on the conditioned media. The size of gel area was measured every day. Vertical axis: gel size as percentage of initial area; horizontal axis, time after release (day). Data shown are means ± SEM for representative data from three separate experiments. Each experiments for contraction in triplicate. ($^*p < 0.05$).

content of the wound matrix is much higher than that of the adjacent tissue.[23] It is reasonable for fibroblast and inflammatory cells, such as neutrophil and monocyte, to migrate into the wound area.[24–28] Recruiting the inflammatory cells is important for management of infection and removal of tissue debris in the wound area. Fibronectin helps platelet to attach to collagen[29] and enmeshed in blood clots[28] at the defect of tissue. Moreover fibronectin mediate fibroblasts attachment to collagen.[30] Taken together, these findings suggest that fibronectin is very important for wound healing.

Our data clearly showed that CAM inhibited the migration of even the stimulated fibroblast by TXA_2 analog U46619.

TXA_2 is an inflammatory mediator that can modulate a variety of important biologic functions, including coagulation and vasomotor and bronchomotor reactivity.[31] Several report shows that adequate physiologic concentration of U46619 (TXA_2 analog) is 10^{-8}–10^{-6} M.[32,33] Our previous study showed that 2×10^{-7} nM of U46619 showed highest activity of fibroblast migration,[34] then we chose this concentration for stimulator of migration.

Clarithromycin had no effect on fibroblast contraction which is another function and final process of wound healing. Not like other drugs which effect on fibroblast migration,[35,36] CAM effect might be limited in early part of wound healing process.

The mechanism of CAM effect on the fibroblast migration is not clear. Previous studies demonstrate that several mediators that inhibit the lung fibroblast migration are related to the protein kinase A (PKA).[17,37] The current study indicated that CAM effect but PGD_2 on HFL-1 migration was related to protein kinase A (Fig. 9). We had also tried but fail to show the effect of CAM on the p38 activity that is related to cell migration[38] (data not shown). Continuous study of CAM mechanism would be required.

There are no clinical trials with CAM for treatment of fibroblast related to wound healing such as IPF. However, there are in vivo experiment reports which show macrolide effects on mouse models of idiopathic pulmonary fibrosis. Fourteen-membered ring macrolides inhibit bleomycin-induced acute lung injury.[39,40] Recent studies have shown that both COPD and asthma are also associated with fibrosis of small airways.[41,42] We might be able to expand the treatment territory with CAM even to COPD and asthma, and to use CAM. There is a possibility of using CAM for treatment of these diseases.

In summary, the current study demonstrated that clarithromycin could inhibit fibroblast migration. This effect of CAM could potentially reduce the tissue remodeling and relieve the diseases of fibrotic.

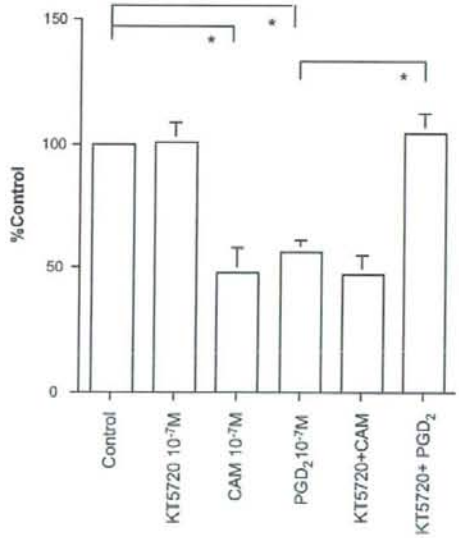

Figure 9 Effect of protein kinase A inhibitor on CAM reducing HFL-1 migration. HFL-1 migration was performed in the Boyden blind well chamber assay system. Protein kinase A inhibitor KT5720 was added to the upper wells with or without CAM. KT5720 effect on PGD_2 was the positive control of this assay. ($^*p < 0.05$).

Conflict of interest and sources of funding

The authors declare that they had no conflict of interest.

Acknowledgements

The authors thank Miss Makiko Kase for her excellent technical assistance.

References

1. Rennard SI, Jaurand MC, Bignon J, Kawanami O, Ferrans VJ, Davidson J, et al. Role of pleural mesothelial cells in the

Please cite this article in press as: Kohyama T et al., Clarithromycin inhibits fibroblast migration, Respiratory Medicine (2008), doi:10.1016/j.rmed.2008.06.020

production of the submesothelial connective tissue matrix of lung. *Am Rev Respir Dis* 1984;**130**:267–74.
2. Kudoh S, Azuma A, Yamamoto M, Izumi T, Ando M. Improvement of survival in patients with diffuse panbronchiolitis treated with low-dose erythromycin. *Am J Respir Crit Care Med* 1998;**157**:1829–32.
3. Pukhalsky AL, Shmarina GV, Kapranov NI, Kokarovtseva SN, Pukhalskaya D, Kashirskaja NJ. Anti-inflammatory and immunomodulating effects of clarithromycin in patients with cystic fibrosis lung disease. *Mediators Inflamm* 2004;**13**:111–7.
4. Takizawa H, Desaki M, Ohtoshi T, Kikutani T, Okazaki H, Sato M, et al. Erythromycin suppresses interleukin 6 expression by human bronchial epithelial cells: a potential mechanism of its anti-inflammatory action. *Biochem Biophys Res Commun* 1995;**210**:781–6.
5. Takizawa H, Desaki M, Ohtoshi T, Kawasaki S, Kohyama T, Sato M, et al. Erythromycin modulates IL-8 expression in normal and inflamed human bronchial epithelial cells. *Am J Respir Crit Care Med* 1997;**156**:266–71.
6. Kohyama T, Takizawa H, Kawasaki S, Akiyama N, Sato M, Ito K. Fourteen-member macrolides inhibit interleukin-8 release by human eosinophils from atopic donors. *Antimicrob Agents Chemother* 1999;**43**:907–11.
7. Sasaki M, Ito T, Kashima M, Fukui S, Izumiyama N, Watanabe A, et al. Erythromycin and clarithromycin modulation of growth factor-induced expression of heparanase mRNA on human lung cancer cells in vitro. *Mediators Inflamm* 2001;**10**:259–67.
8. Mikasa K, Sawaki M, Kita E, Hamada K, Teramoto S, Sakamoto M, et al. Significant survival benefit to patients with advanced non-small-cell lung cancer from treatment with clarithromycin. *Chemotherapy* 1997;**43**:288–96.
9. Sakamoto M, Mikasa K, Majima T, Hamada K, Konishi M, Maeda K, et al. Anti-cachectic effect of clarithromycin for patients with unresectable non-small cell lung cancer. *Chemotherapy* 2001;**47**:444–51.
10. Li Y, Azuma A, Takahashi S, Usuki J, Matsuda K, Aoyama A, et al. Fourteen-membered ring macrolides inhibit vascular cell adhesion molecule 1 messenger RNA induction and leukocyte migration: role in preventing lung injury and fibrosis in bleomycin-challenged mice. *Chest* 2002;**122**:2137–45.
11. Watanabe A, Anzai Y, Niitsuma K, Saito M, Yanase K, Nakamura M. Penetration of minocycline hydrochloride into lung tissue and sputum. *Chemotherapy* 2001;**47**:1–9.
12. Morris DL, De Souza A, Jones JA, Morgan WE. High and prolonged pulmonary tissue concentrations of azithromycin following a single oral dose. *Eur J Clin Microbiol Infect Dis* 1991;**10**:859–61.
13. Boyden S. The chemotactic effect of mixtures of antibody and antigen on polymorphonuclear leucocytes. *J Exp Med* 1962; **115**:453–66.
14. Bell E, Ivarsson B, Merrill C. Production of a tissue-like structure by contraction of collagen lattices by human fibroblasts of different proliferative potential in vitro. *Proc Natl Acad Sci U S A* 1979;**76**:1274–8.
15. Mio T, Adachi Y, Romberger DJ, Ertl RF, Rennard SI. Regulation of fibroblast proliferation in three dimensional collagen gel matrix. *In Vitro Cell Dev Biol* 1996;**32**:427–33.
16. Elsdale T, Bard J. Collagen substrata for studies on cell behavior. *J Cell Biol* 1972;**54**:626–37.
17. Kohyama T, Ertl RF, Valenti V, Spurzem J, Kawamoto M, Nakamura Y, et al. Prostaglandin E(2) inhibits fibroblast chemotaxis. *Am J Physiol Lung Cell Mol Physiol* 2001;**281**: L1257–63.
18. Kohyama T, Liu XD, Wen FQ, Kim HJ, Takizawa H, Rennard SI. Prostaglandin D2 inhibits fibroblast migration. *Eur Respir J* 2002;**19**:684–9.
19. Hunninghake WC, Garret KC, Richerson HB, Fantone JC, Ward PA, Rennard SI, et al. Pathogenesis of the granulomatous lung disease (state of art). *Am Rev Respir Dis* 1984;**130**: 476–96.
20. Panos RJ, Mortenson RL, Niccoli SA, King Jr TE. Clinical deterioration in patients with idiopathic pulmonary fibrosis: causes and assessment. *Am J Med* 1990;**88**:396–404.
21. King Jr TE, Schwarz MI, Brown K, Tooze JA, Colby TV, Waldron Jr JA, et al. Idiopathic pulmonary fibrosis: relationship between histopathologic features and mortality. *Am J Respir Crit Care Med* 2001;**164**:1025–32.
22. Adachi Y, Mio T, Takigawa K, Striz I, Romberger DJ, Spurzem JR, et al. Fibronectin production by cultured human lung fibroblasts in three-dimensional collagen gel culture. *In Vitro Cell Dev Biol Anim* 1998;34:203–10.
23. Grinnell F, Billingham RE, Burgess L. Distribution of fibronectin during wound healing in vivo. *J Invest Dermatol* 1981;**76**: 181–9.
24. Gauss-Muller V, Kleinman HK, Martin GR, Schiffmann E. Role of attachment factors and attractants in fibroblast chemotaxis. *J Lab Clin Med* 1980;**96**:1071–80.
25. Postlethwaite AE, Keski-Oja J, Balian G, Kang AH. Induction of fibroblast chemotaxis by fibronectin. Localization of the chemotactic region to a 140,000-molecular weight non-gelatin-binding fragment. *J Exp Med* 1981;**153**:494–9.
26. Doillon CJ, Silver FH. Collagen-based wound dressing: effects of hyaluronic acid and fibronectin on wound healing. *Biomaterials* 1986;**7**:3–8.
27. Jarstrand C, Ahlgren T, Berghem L. Fibronectin increases the motility, phagocytosis and NBT (nitroblue tetrazolium)-reduction of granulocytes. *J Clin Lab Immunol* 1982;**8**:59–63.
28. Grinnell F. Fibronectin and wound healing. *J Cell Biochem* 1984;**26**:107–16.
29. Hynes RO, Ali IU, Destree AT, Mautner V, Perkins ME, Senger DR, et al. A large glycoprotein lost from the surfaces of transformed cells. *Ann N Y Acad Sci* 1978;**312**:317–42.
30. Rennard SI, Chen YF, Robbins RA, Gadek JE, Crystal RG. Fibronectin mediates cell attachment to C1q: a mechanism for the localization of fibrosis in inflammatory disease. *Clin Exp Immunol* 1983;**54**:239–47.
31. Ogletree ML. Overview of physiological and pathophysiological effects of thromboxane A2. *Fed Proc* 1987;**46**:133–8.
32. Mene P, Abboud HE, Dunn MJ. Regulation of human mesangial cell growth in culture by thromboxane A2 and prostacyclin. *Kidney Int* 1990;**38**:232–9.
33. Studer RK, Craven PA, DeRubertis FR. Thromboxane stimulation of mesangial cell fibronectin synthesis is signalled by protein kinase C and modulated by cGMP. *Kidney Int* 1994; **46**:1074–82.
34. Kohyama T, Liu X, Wen FQ, Kim HJ, Takizawa H, Rennard SI. Potentiation of human lung fibroblast chemotaxis by the thromboxane A(2) analog U-46619. *J Lab Clin Med* 2002;**139**: 43–9.
35. Kohyama T, Wyatt TA, Liu X, Wen FQ, Kobayashi T, Fang Q, et al. PGD2 modulates fibroblast-mediated native collagen gel contraction. *Am J Respir Cell Mol Biol* 2002; **27**:375–81.
36. Kohyama T, Liu X, Wen FQ, Zhu YK, Wang H, Kim HJ, et al. PDE4 inhibitors attenuate fibroblast chemotaxis and contraction of native collagen gels. *Am J Respir Cell Mol Biol* 2002;**26**:694–701.
37. Kohyama T, Liu X, Kim HJ, Kobayashi T, Ertl RF, Wen FQ, et al. Prostacyclin analogs inhibit fibroblast migration. *Am J Physiol Lung Cell Mol Physiol* 2002;**283**:L428–32.
38. Heuertz RM, Tricomi SM, Ezekiel UR, Webster RO. C-reactive protein inhibits chemotactic peptide-induced p38 mitogen-activated protein kinase activity and human neutrophil movement. *J Biol Chem* 1999;**274**:17968–74.
39. Azuma M, Nishioka Y, Aono Y, Inayama M, Makino H, Kishi J, et al. Role of alpha1-acid glycoprotein in therapeutic antifibrotic

Please cite this article in press as: Kohyama T et al., Clarithromycin inhibits fibroblast migration, Respiratory Medicine (2008), doi:10.1016/j.rmed.2008.06.020

effects of imatinib with macrolides in mice. *Am J Respir Crit Care Med* 2007;**176**:1243–50.
40. Kawashima M, yatsunami J, Fukuno Y, Nagata M, Tominaga M, Hayashi S. Inhibitory effects of 14-membered ring macrolide antibiotics on bleomycin-induced acute lung injury. *Lung* 2002;**180**:73–89.
41. Hoshino M, Nakamura Y, Sim J, Shimojo J, Isogai S. Bronchial subepithelial fibrosis and expression of matrix metalloproteinase-9 in asthmatic airway inflammation. *J Allergy Clin Immunol* 1998;**102**:783–8.
42. Saetta M, Turato G. Airway pathology in asthma. *Eur Respir J Suppl* 2001;**34**:18s–23s.

Please cite this article in press as: Kohyama T et al., Clarithromycin inhibits fibroblast migration, Respiratory Medicine (2008), doi:10.1016/j.rmed.2008.06.020